Development and characterization of the first selective class IIb histone deacetylase degraders

Shiyang Zhai,[a] Linda Schäker-Hübner,[a] Maria Hanl,[a] Lukas Jacobi,[b] Dominika Ewa Pieńkowska, [c] Jan Gerhartz,[c] Rabea Voget,[d] Michael Gütschow,[d] Felix Meissner,[b] Radosław P. Nowak,[c] Christian Steinebach,[d] Finn K. Hansen[a]*

[a] Department of Pharmaceutical and Cell Biological Chemistry, Pharmaceutical Institute, University of Bonn, Bonn, Germany.

[b] Institute of Innate Immunity, Department of Systems Immunology and Proteomics, Medical Faculty, University of Bonn, Bonn, Germany.

[c] Institute of Structural Biology, Medical Faculty, University of Bonn, Bonn, Germany.

[d] Department of Pharmaceutical and Medicinal Chemistry, Pharmaceutical Institute, University of Bonn, Bonn, Germany.

Abstract

Proteolysis-targeting chimeras (PROTACs) are emerging new therapeutic modalities that facilitate the targeted degradation of disease-relevant proteins *via* an event-driven mode of action. In this work, we report the design, synthesis, and biological evaluation of the first-in-class selective degraders of the class IIb histone deacetylases (HDACs) 6 and 10. To this end, the dual HDAC6/10 inhibitor Tubastatin A and a ring-opened analog were connected *via* well-established PROTAC linkers to pomalidomide and phenylglutarimides as cereblon recruiters. This approach led to the discovery of **AP1** (HDAC6 DC_{50} = 13 nM; HDAC10 DC_{50} = 29 nM) as a potent degrader of class IIb HDACs. Importantly, **AP1** did neither degrade HDAC1/8 (class I) and HDAC4 (class IIa), nor did it induce histone H3 hyperacetylation, thereby confirming its selectivity for class IIb HDACs. Due to its low cytotoxicity against hematological and solid cancer cell lines, **AP1** represents a valuable tool compound for the chemical knockdown of class IIb HDACs.

Introduction

Protein acetylation, a critical post-translational modification, regulates crucial cellular processes such as enzymatic activity, subcellular localization, and protein interactions. Moreover, it impacts cell signaling, turnover, differentiation, and survival.[1] In this process, histone acetyltransferases (HATs) transfer acetyl groups (acetylation), and histone deacetylases (HDACs) remove them (deacetylation), thereby influencing both histone and non-histone proteins in various cellular functions.[2, 3] As essential epigenetic regulators, HDACs have captured significant attention through extensive research spanning multiple stages of tumor development over the past decades, with their dysregulation contributing to tumorigenesis.[1-3]

Mammalian HDACs, 18 subtypes in total, were categorized into four classes based on their sequences, structural features, and cellular localization, among which, class I (HDAC1, 2, 3 and 8), class II (HDAC4, 5, 7, 9, 6 and 10), and class IV (HDAC11) are Zn^{2+}-dependent. In contrast, members of class III (Sirt1-7) depend on NAD^{+}. Class II HDACs can be further divided into class IIa (HDAC4, 5, 7, and 9) and class IIb (HDAC6 and 10). Notably, the key characteristics of class IIb HDACs are that they are primarily located in the cytoplasm and have acetylated non-histone proteins as primary substrates.[4] Substantial progress has been made to develop efficacious HDAC inhibitors (HDACi) to combat various HDAC-related diseases, including cancer. To date, four HDACi have been approved by the FDA for diverse cancer treatments.[3, 5] However, despite their promising impact on cancer growth, the widespread use of non-selective HDACi is associated with various side effects.[5] This underscores the need for exploring more targeted approaches to achieve subtype- or class-selective HDAC inactivation, aiming for both efficacy and enhanced safety in therapeutic interventions. To this end, class IIb HDACs gained much attention.

HDAC6, as one of the Zn^{2+}-dependent Class IIb members, can regulate various biological processes *via* its deacetylation activity on acetylated lysines in non-histone proteins, such as cellular proliferation, motility, apoptosis, DNA damage response, activation of heat shock response, transcriptional repression as well as metabolic response.[1] Beyond deacetylation, HDAC6 can also contribute to cellular processes like protecting against stress-induced protein aggregation and facilitating the transport of ubiquitinated proteins via the zinc-finger ubiquitin-binding domain (UBD) and a dynein-binding domain in its structure.[1] Since HDAC6 participates in several biological processes *via* different enzymological and non-enzymological functions, the continuous development of inhibitors and degraders for HDAC6 has emerged as a hot topic[6-16].

HDAC10, the other member of class IIb, functions as a potent polyamine deacetylase with a notable preference for N^8-acetylspermidine hydrolysis over acetylated lysine.[17-20] Importantly, HDAC10 plays a significant role in various biological processes related to cancer, such as cellular proliferation, apoptosis, invasion, autophagy, and drug resistance.[21] Notably, its involvement in promoting cellular survival through autophagy has been extensively reported in instances such as neuroblastoma and ovarian cancer.[21] From the aspect of drug resistance, elevated HDAC10 levels are associated with protecting cancer cells from chemotherapy. Notably, HDAC10 inhibition enhances cancer cell sensitivity to chemotherapy.[21] These findings underscore the potential of HDAC10 as a promising therapeutic target in cancer treatment.

Structurally distinctive within the Zn^{2+}-dependent HDAC family, HDAC6 and HDAC10 feature two deacetylase domains. In HDAC6, both domains are active with different functions: deacetylase domain 1 (DD1) focuses on deacetylating substrates with acetylated lysine at their C terminus,[1] while deacetylase domain 2 (DD2) exclusively targets peptides featuring an internal acetylated lysine residue. Conversely,

HDAC10 possesses an active polyamine deacetylase (PDAC) domain and an inactive pseudodeacetylase (ΨDAC) domain.[17-20] Key residues in the active site of HDAC10, such as the tandem histidine and E274 (zebrafish), contribute to its specificity for polyamine substrates.[17-20] The unique ηA2 helix and a specific loop induce steric constriction in the active site, thereby influencing its deacetylase activities.[17-20] Despite differences in substrate selectivity, crystal structures reveal a typical assembly pattern for HDAC6 and HDAC10,[17-20] opening avenues for developing molecular tools to achieve dual inactivation for both targets.

In contrast to the occupancy-driven pharmacology of classical inhibitors, proteolysis-targeting chimeras (PROTACs) represent a small molecule-based heterobifunctional tool with an event-driven mode of action (MoA). This catalytic MoA relies on hijacking the endogenous ubiquitination process in cells, thereby tagging the protein of interest (POI) for degradation by the proteasome.[22] Consequently, PROTAC-induced degradation reduces cellular POI levels, offering potential therapeutic applications across various diseases.

In this study, we developed a series of class IIb HDAC PROTACs using Tubastatin A derivatives as HDAC class IIb warheads, connected *via* suitable PROTAC spacers to pomalidomide or phenylglutarimides as cereblon (CRBN)-recruiters.

RESULTS AND DISCUSSION

Molecular Docking analysis and design

To design a PROTAC molecule and determine the optimal linker location, we first analyzed the binding mode of Tubastatin A. According to the elucidated crystal structures of HDAC6 (PDB: 6THV)[23] and HDAC10 (PDB: 6WBQ)[24] in complex with Tubastatin A, it is evident that Tubastatin A exhibits a

notable capacity for effective interaction with both targets within their respective catalytic pockets. In the case of HDAC6 (**Fig. 1A**), the hydroxamic acid group of Tubastatin A establishes a hydrogen bond with residue H574 and engages in chelation with the Zn^{2+} ion within the catalytic tunnel. Similarly, for HDAC10 (**Fig. 1B**), interactions of the hydroxamic acid group with His136 and His137, alongside chelation with the Zn^{2+} ion, are also observed. The tricyclic tetrahydro-γ-carboline capping group of Tubastatin A has been shown to interact with residues E24 and W205. In contrast, the residue E274 can form electrostatic interactions with the tertiary amine in the capping group. Notably, E24 and E274 are critical for HDAC10 selectivity, facilitating the deep insertion of Tubastatin A into the HDAC10 catalytic pocket. In light of these documented observations, Tubastatin A emerges as a promising ligand candidate for developing dual degraders targeting both class IIb HDACs.

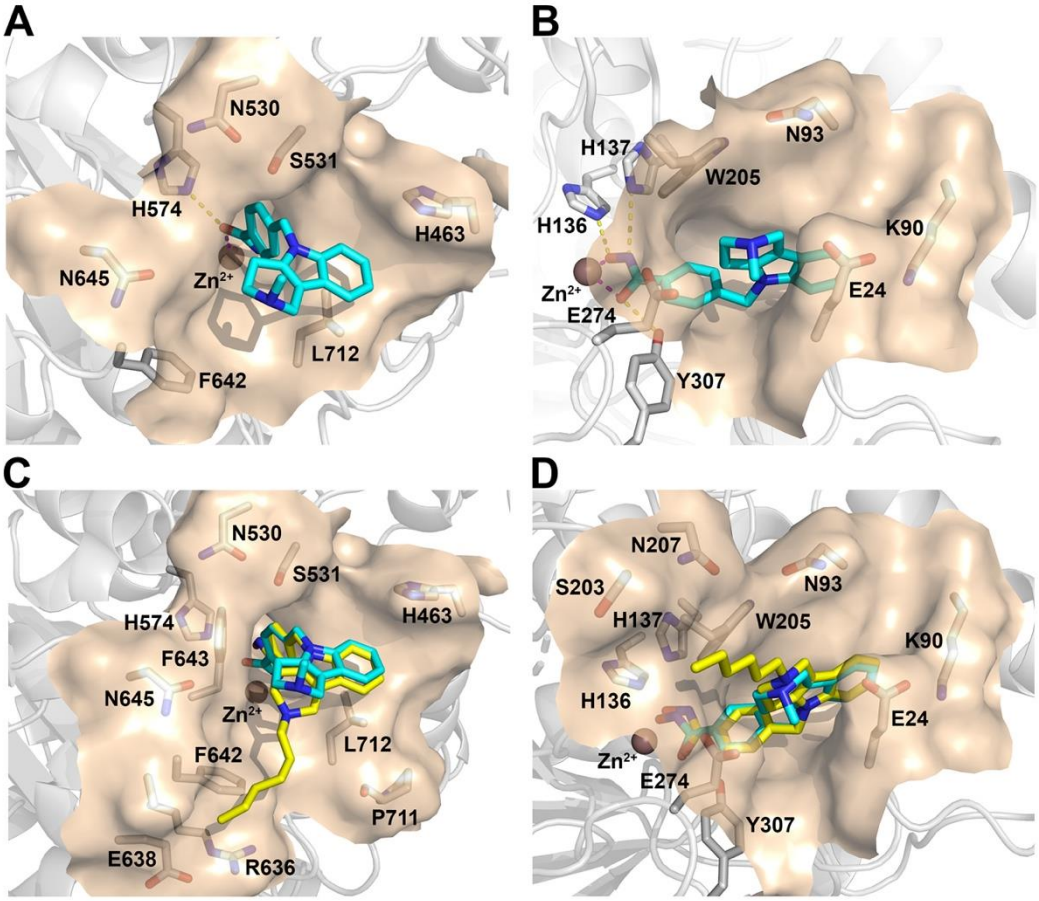

Figure 1. (A, B) Binding mode of Tubastatin A (cyan) in HDAC6 (A; PDB: 6THV) and HDAC10 (B; PDB: 6WBQ). (C, D) Docking pose of the Tubastatin A derivative in HDAC6 (C) and HDAC10 (D). Hydrogen bonds are indicated by yellow dashes, and the metal chelation interaction is indicated by purple dashes.

To determine the optimal anchor point on Tubastatin A for the attachment of PROTAC linkers, as illustrated in **Figure 1A**, an analysis of Tubastatin A's conformation within HDAC6 reveals multiple possibilities in the capping group for linker extension, specifically at positions C1, C6, as well as on the tertiary amine. In contrast, for HDAC10 (**Figure 1B**), both C1 and C6 are buried into the pocket, which may increase the probability of collisions between the linker-attached ligand and nearby residues, such as E24 and K90. Therefore, a Tubastatin A derivative featuring a flexible hexyl chain attached to the tertiary amine, designed to mimic the PROTAC linker, was docked into the catalytic pockets of both HDAC6 and HDAC10 (**Figure 1C** and **1D**). Notably, this derivative aligns well with the co-crystal structures of Tubastatin A bound to both HDAC6 and HDAC10, with the hexyl chain extending beyond the pocket boundaries in both cases. Consequently, the tertiary amine in the capping group of Tubastatin A was identified as an optimal anchor point.

A PROTAC molecule typically comprises a POI warhead, an E3 ligase recruiter, and a linker to connect both ligands. In contrast to Tubastatin A, acknowledged for its enhanced selectivity toward HDAC10 relative to HDAC6 (8-fold), a bicyclic derivative featuring a dimethylamine moiety in the capping group demonstrated even greater selectivity, reaching up to 40-fold.[25] Consequently, as shown in **Figure 2**, Tubastatin A and its bicyclic derivative were utilized as warheads in the present study. The flexible alkyl chain, as a commonly reported linker type, was employed in the design. Furthermore, since the variation of the E3 ligase ligand has been shown to impact degrader activity as well as stability[26], two

different CRBN ligands, specifically pomalidomide and a phenylglutarimide derivative, were chosen as E3 ligase recruiters.

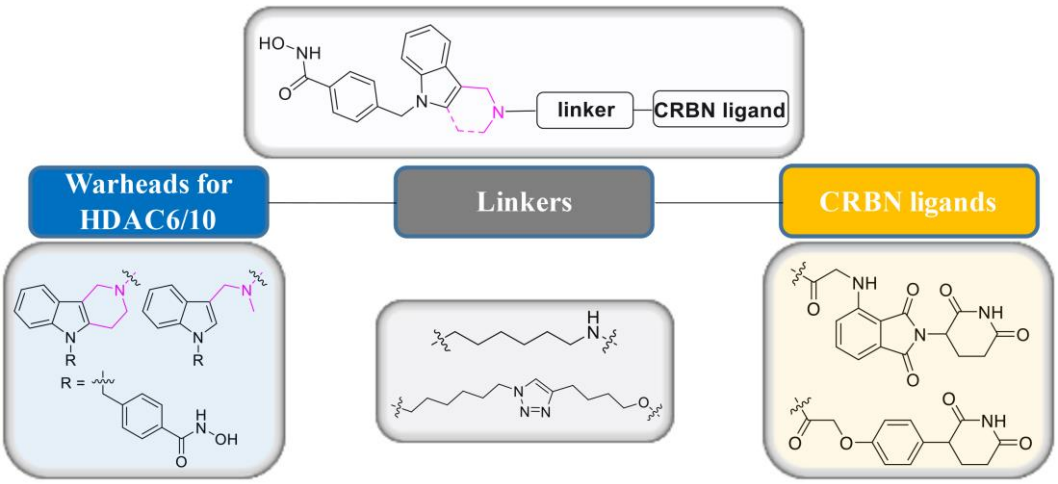

Figure 2. Design of potential class IIb HDAC degraders.

Chemistry

Scheme 1 illustrates the synthesis of protected POI ligands with the attached linkers and the synthesis of CRBN ligands. Briefly, to synthesize compounds **4** and **5** (**Scheme 1A**), commercially available phenylhydrazine and *tert*-butyl 4-oxopiperidine-1-carboxylate were used as starting materials to generate tricyclic compound **1**. Subsequently, the alkylation of the indole with methyl 4-(bromomethyl)benzoate afforded compound **2**. Compound **2** was hydrolyzed with lithium hydroxide monohydrate and acidified with hydrochloric acid to release the carboxylic acid group. The resulting compound was subjected to a HATU-mediated amide coupling reaction with *O*-benzylhydroxylamine hydrochloride to yield compound **3**. Subsequently, the Boc-protecting group in compound **3** was removed with trifluoroacetic

acid (TFA). The released secondary amine was then alkylated with *tert*-butyl (6-bromohexyl)carbamate to furnish compound **4** and 1-azido-6-bromohexane to generate compound **5**.

For the synthesis of the bicyclic warhead compound **9** (**Scheme 1B**), a previously reported method was employed[25]. Starting from the commercially available 1*H*-indole-3-carbaldehyde, a substitution reaction was performed to provide compound **6**. In the next step, the reductive amination of **6** with methylamine afforded **7**. Afterward, the secondary amine of compound **7** was substituted with *tert*-butyl (6-bromohexyl)carbamate to yield compound **8**. Following the hydrolysis of methyl ester in compound **8** and subsequent acidification to form the carboxylic acid moiety, the *O*-benzyl-protected compound **9** was generated through a HATU-mediated amide coupling reaction.

The synthesis of CRBN ligands is summarized in **Scheme 1C**. The pomalidomide-based intermediate **10**[27] and the phenylglutarimide building block **13**[26] were synthesized following previously reported methods. The carboxylic acid products of compounds **10** and **13** were obtained by the deprotection reactions using TFA. Subsequently, compounds **12** and **15** were synthesized *via* HATU-mediated esterification of **11** and **14** with hex-5-yn-1-ol.

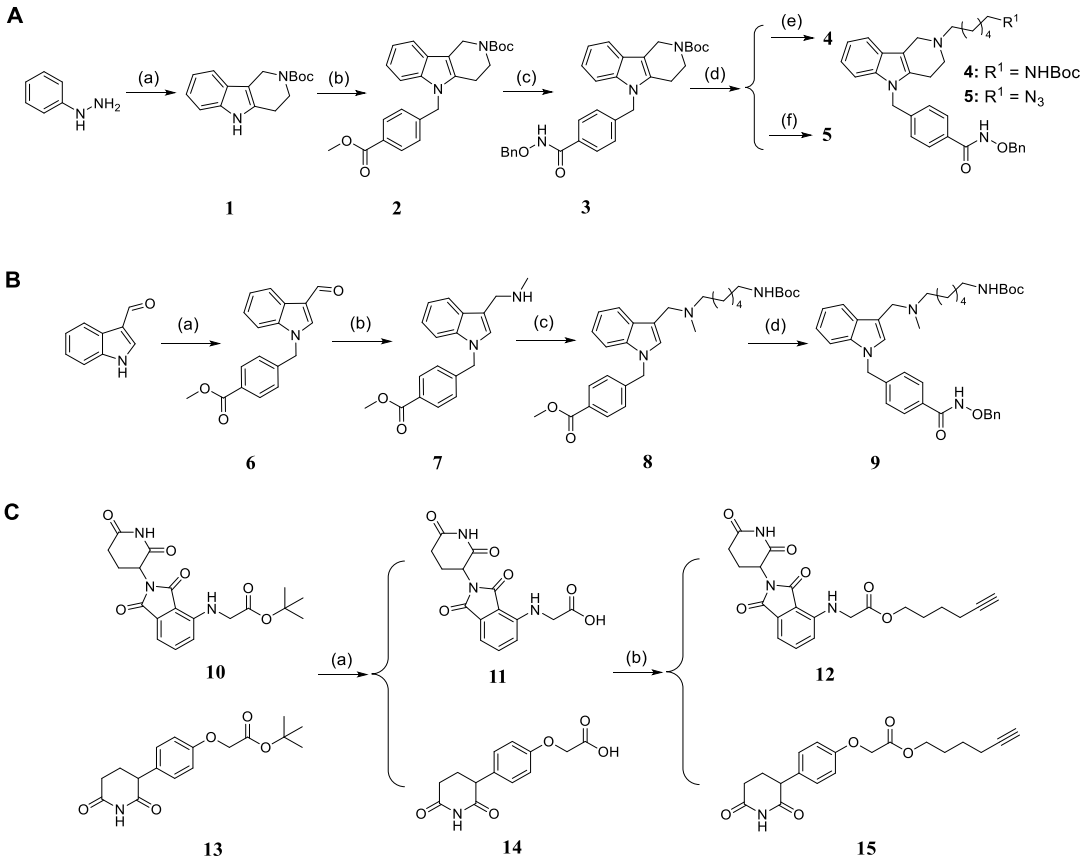

Scheme 1. Synthesis of the protected POI ligands with attached linkers and CRBN ligands. **A**: (a) *tert*-butyl 4-oxopiperidine-1-carboxylate, 2,4,6-tripropyl-1,3,5,2,4,6-trioxatriphosphinane 2,4,6-trioxide (50% solution in EtOAc), toluene, 90 °C, 16 h, 60%; (b) methyl 4-(bromomethyl)benzoate, Cs_2CO_3, ACN, reflux, 15 h, 57% [28]; (c) (i) LiOH × H_2O, THF/MeOH/H_2O, rt, 17 h; (ii) HCl (0.5 M in H_2O); (iii) *O*-benzylhydroxylamine hydrochloride, HATU, DIPEA, anhydrous DMF, rt, 16 h, 75% (three steps); (d) TFA, CH_2Cl_2, rt, 2 h; (e) *tert*-butyl (6-bromohexyl)carbamate, K_2CO_3, anhydrous DMF, rt, 18 h, 66% (two steps); (f) 1-azido-6-bromohexane, K_2CO_3, anhydrous DMF, rt, 20 h, 71% (two steps); **B**: (a) methyl 4-(bromomethyl)benzoate, Cs_2CO_3, ACN, reflux, 15 h, 99% [28]; (b) (i) $MeNH_2$, MeOH, rt, 19 h; (ii) $NaBH_4$, MeOH, 0 °C to rt, 3 h, 87% (two steps) [25, 29]; (c) *tert*-butyl (6-bromohexyl)carbamate, K_2CO_3, anhydrous DMF, rt, 15 h, 67%; (d) (i) LiOH × H_2O, THF/MeOH/H_2O, rt, 16.5 h; (ii) HCl (0.5 M in H_2O); (iii) *O*-benzylhydroxylamine hydrochloride, HATU, DIPEA, anhydrous DMF, rt, 17 h, 80% (three

steps); **C**: (a) TFA, CH_2Cl_2, rt, 2 h; (b) hex-5-yn-1-ol, HATU, DIPEA, anhydrous DMF, rt, 15 h, 55% (compound **12**), 69% (compound **15**).

Following the synthesis of linker-attached warhead ligands and E3 ligase recruiters, the final key intermediates for PROTACs were synthesized using either amide coupling reactions or Cu(I)-catalyzed azide-alkyne cycloadditions. **Scheme 2** displays the synthesis of PROTACs **AP1-AP6**. Briefly, the *tert*-butyloxycarbonyl protecting group in compound **4** was removed with TFA. Afterward, amide coupling reactions with HATU and DIPEA in anhydrous DMF were carried out between de-protected compound **4** and compound **11** or **14**, leading to the formation of compounds **16** and **17**, respectively. The same procedure was used to generate compounds **20** and **21**. For compound **5**, featuring an azide group at the linker terminus, Cu(I)-catalyzed azide-alkyne cycloaddition reactions[30] were carried out to afford compounds **18** and **19**. Afterward, the benzyl protecting groups in compounds **16-21** were removed under a hydrogen atmosphere using Pd/C (5%) as a catalyst to release the zinc-binding groups and to furnish the desired PROTACs **AP1-AP6**.

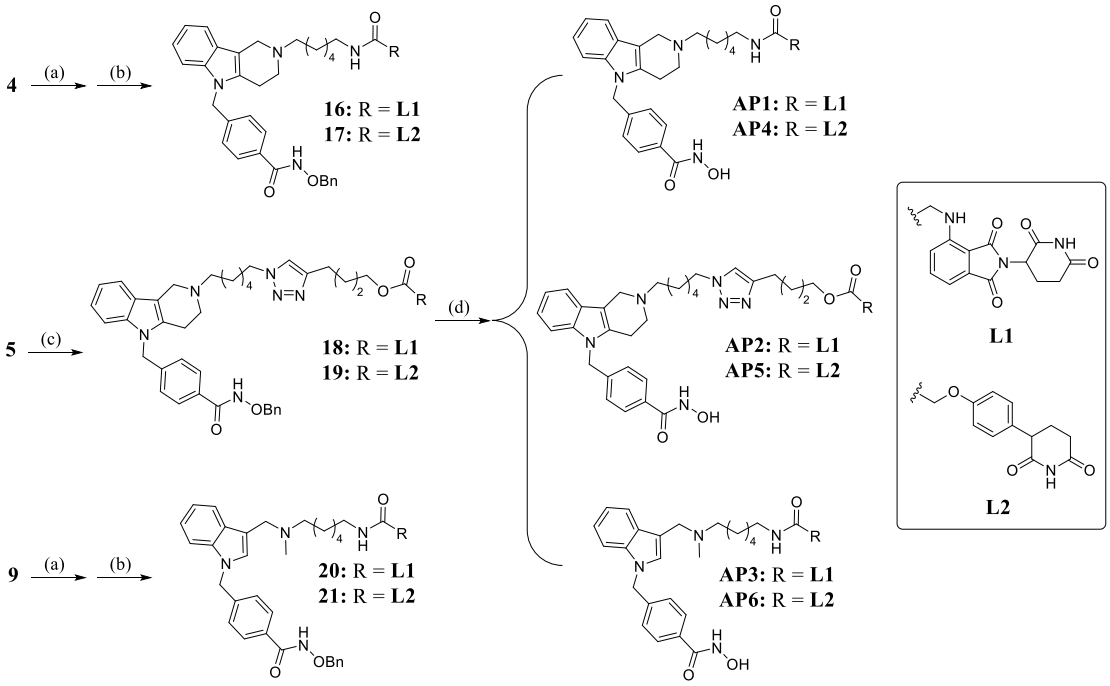

Scheme 2. Synthesis of PROTACs **AP1**-**AP6**. (a) TFA, CH_2Cl_2, rt, 2 h; (b) compound **11** or **14**, HATU, DIPEA, anhydrous DMF, rt, 17 h, 54-88% (two steps); (c) compound **12** or **15**, ascorbic acid, $CuSO_4$, DMF/H_2O (10:1), rt, 2-4 h, 54-59%; (d) H_2, Pd/C, EtOH/MeOH, rt, overnight, 9-33%.

Targets engagement assays and evaluation of physicochemical properties

All synthesized PROTACs were evaluated for their *in vitro* inhibitory activity against HDAC6 and HDAC10 using fluorogenic enzyme inhibition assays with Z-Lys(Ac)-AMC or Ac-spermidine-AMC as substrates. The results are summarized in **Table 1**. All compounds exhibited potent inhibitory activities with IC_{50} values in the double- or even single-digit nanomolar concentration range, indicating effective target engagement of both class IIb HDACs *in vitro*. Next, we performed cellular CRBN target engagement studies using a NanoBRET assay. As previously published, HEK293T cells stably expressing NanoLuc-CRBN were used for competition experiments with a BODIPY-lenalidomide tracer[31]. All PROTACs demonstrated IC_{50} values in a single- or double-digit micromolar range, verifying CRBN target engagement and cell permeability. Consistent with previous reports[32], we noticed that some pomalidomide-based PROTACs showed autofluorescence signal at high concentrations in the NanoBRET assay. The compounds affected with high background fluorescence are indicated with an asterisk in the **Table 1**, where the IC_{50} represents an upper estimate. An overview of the physicochemical properties of the synthesized degraders is provided in **Table 1** to assess their drug-likeness. In general, PROTACs **AP1** to **AP6** are characterized by a moderate molecular weight, lipophilicity (partition coefficients were experimentally determined by an HPLC method), and polar surface area. As expected, the cyclization of the HDAC warhead in **AP1**, **AP2**, **AP4**, and **AP5** led to a somewhat higher logD value. In general, representatives of the pomalidomide-based series (L1) are slightly more lipophilic than their

phenylglutarimide counterparts. PROTACs **AP1** to **AP6** are tightly bound to plasma proteins as indicated by the experimentally determined binding to human serum albumin (fu < 0.05), which is, however, a common feature of degraders with linear rotatable linkers.[33]

Table 1. Evaluation of **AP1-AP6** for target engagement and physicochemical properties.

Cmpd.	IC_{50} (µM)			M_r (g/mol)	elog $D_{7.4}$[c]	TPSA (Å^2)[d]	PPB (%)[e]	NRotB[f]
	HDAC6[a]	HDAC10[b]	CRBN					
AP1	0.040 ± 0.005	0.022 ± 0.003	*7.5	374	1.8	182.18	96.7	16
AP2	0.047 ± 0.003	0.017 ± 0.003	*4.4	434	2.3	210.09	96.7	21
AP3	0.026 ± 0.002	0.007 ± 0.001	*80.8	394	1.3	182.18	97	18
AP4	0.025 ± 0.0005	0.023 ± 0.003	2.2	302	1.6	142.00	96.3	16
AP5	0.049 ± 0.005	0.015 ± 0.002	2.5	360	2.2	169.91	96.7	21
AP6	0.031 ± 0.0005	0.012 ± 0.004	15.6	310	1.2	142.00	96.1	18
Vorinostat	0.033 ± 0.003	n.d.	n.d.	n.d.	n.d.	n.d.	n.d.	n.d.
Quisinostat	0.105 ± 0.009	0.005 ± 0.0004	n.d.	n.d.	n.d.	n.d.	n.d.	n.d.
Lenalidomide	n.d.	n.d.	0.6	n.d.	n.d.	n.d.	n.d.	n.d.

[a]Z-Lys(Ac)-AMC was used as substrate; [b]Ac-spermidine-AMC was used as substrate; [c]Distribution coefficients at pH = 7.4 were estimated by a HPLC-based method; [d] Topological polar surface area is given in Å^2; [e]Plasma protein binding, experimentally determined percentage of compound bound to human serum albumin; [f] NRotB, number of rotatable bonds; n.d.: not determined. Asterisks (*) indicate compounds with high background fluorescence, IC_{50} values should be considered as an upper estimate.

Class IIb HDAC degradation by AP1-AP6

Following the target engagement assays, we evaluated the degradation efficacy of compounds **AP1-AP6**. Western blot analyses of HDAC6 and HDAC10 protein levels were performed after treatment of MM.1S cells with 1 or 5 μM of each PROTAC for 24 h. As shown in **Figure 3A** and **3B**, compounds **AP1**, **AP3**, **AP4**, and **AP6** exhibited robust degradation of both class IIb HDACs, with **AP2** displaying moderate efficacy. In contrast, minimal degradation of both targets was observed in the case of compound **AP5**.

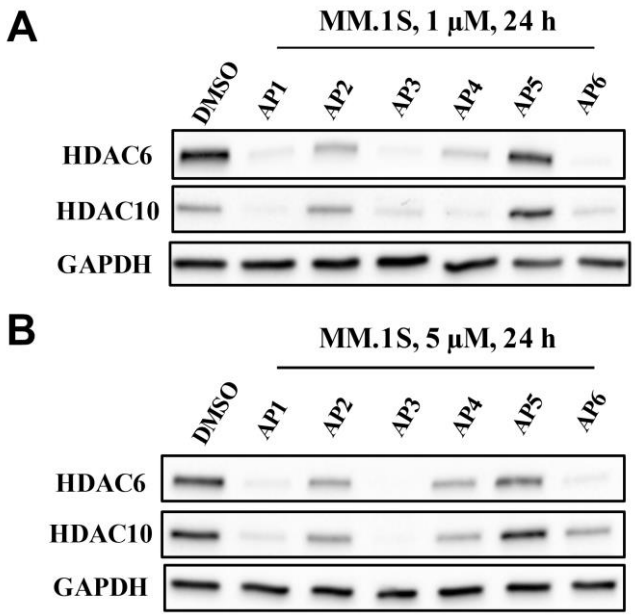

Figure 3. (A, B) Degradation of HDAC6 and HDAC10 mediated by degraders **AP1-AP6** at different concentrations. MM.1S cells were treated with **AP1-AP6** at concentrations of 1 μM (A) and 5 μM (B) for 24 h. HDAC6 and HDAC10 levels were detected by western blot. GAPDH was used as the loading control. Representative images from a total of n = 3 replicates.

The quantified maximal degradation (D_{max}) data are presented in **Table 2**. Notably, compounds **AP1**, **AP3**, **AP4**, and **AP6** exhibited degradation levels of over 80% for both targets at certain concentrations,

except for the HDAC10 degradation under the treatment of **AP6**. **AP1** turned out to be the most efficient dual degrader of this set at 1 μM with D_{max} values of 95% against HDAC6 and 93% against HDAC10, respectively. Conversely, compound **AP2** showed approximately 20% degradation of both targets at 5 μM, while achieving 68% degradation of HDAC6 at 1 μM. However, no degradation of HDAC10 was observed at this concentration. Compound **AP5** demonstrated only slight degradation of both targets at 5 μM, with negligible effects observed at 1 μM. The relatively diminished degradation potencies of compounds **AP2** and **AP5**, when compared with **AP1**, **AP3**, **AP4**, and **AP6**, may be attributed to their longer linkers, potentially affecting the formation of a productive ternary complex.

Table 2. D_{max} and DC_{50} data for HDAC6 and HDAC10 in MM.1S cells after treatment with **AP1**-**AP6** for 24 h.

Cmpd.	HDAC6 Degradation (%)[a]		HDAC10 Degradation (%)[a]		DC_{50} (nM, 24 h)[b]	
	1 μM	5 μM	1 μM	5 μM	HDAC6	HDAC10
AP1	95	96	93	88	13 ± 3.4	29 ± 1.1
AP2	68	24	n.e.	19	n.d.	n.d.
AP3	94	99	85	94	16 ± 3.9	50 ± 2.7
AP4	89	30	84	41	1.3 ± 0.5	1.7 ± 0.9
AP5	n.e.	9	n.e.	3	n.d.	n.d.
AP6	96	95	75	56	4.5 ± 0.4	7.9 ± 3.3

[a]Percentage of degraded HDAC6 or HDAC10 protein after 24 h treatment of MM.1S cells with 1 or 5 μM of each compound, mean of n = 3 replicates; [b]mean ± SD of n = 2 biologically independent experiments, each performed in triplicates; n.d.: not determined; n.e.: no effect (no degradation).

DC_{50} value determination and "hook effect"

To further elucidate the degradation efficiency of the synthesized class IIb HDAC degraders, **AP1**, **AP3**, **AP4** and **AP6** were selected for the determination of their DC_{50} values for HDAC6 and HDAC10 in MM1.S cells (**Figure 4**). As depicted in **Table 2**, all four compounds demonstrated potent DC_{50} values towards HDAC6 and HDAC10. Notably, **AP4** emerged as the most potent degrader for both HDAC6 and HDAC10, with DC_{50} values of 1.3 nM and 1.7 nM, respectively. Furthermore, it is noteworthy that all four compounds exhibited stronger degradation potency towards HDAC6 compared to HDAC10. The most significant difference, reaching 3.1-fold ($DC_{50,\ HDAC10}$ / $DC_{50,\ HDAC6}$), was observed for **AP3** featuring a bicyclic warhead and a pomalidomide-based CRBN ligand. In contrast, the lowest difference of 1.3-fold was observed with **AP4**, comprising Tubastatin A as the POI ligand and a phenylglutarimide derivative-based CRBN ligand. Consistent with the experiments at 1 and 5 μM (**Figure 3**), the phenylglutarimides **AP4** and **AP6** showed a "hook effect". In contrast, the pomalidomide-based PROTACs **AP1** and **AP3** did degrade HDAC6 and HDAC10 in a concentration-dependent manner. Another notable structure-degradation relationship was observed for the Tubastatin A-based degraders **AP1** and **AP4** which demonstrated stronger degradation potency toward class IIb HDACs than the corresponding bicyclic derivative-based degraders (see **AP1** *vs.* **AP3** and **AP4** *vs.* **AP6**; see **Table 2** and **Figure 4**). When comparing the degradation efficacy of the pomalidomide-based degraders with the phenylglutarimides, it is evident that the phenylglutarimides have lower DC_{50} values (see **AP1** *vs.* **AP4** and **AP3** *vs.* **AP6**; see **Table 2** and **Figure 4**). However, this improvement comes at the expense of a prominent "hook effect."

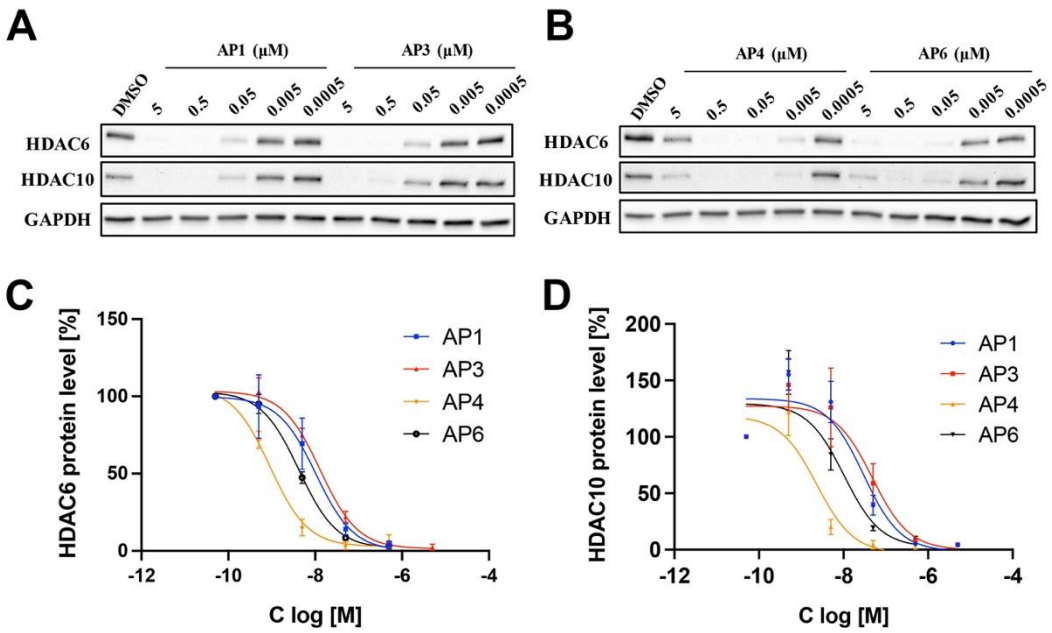

Figure 4. Determination of DC_{50} values of **AP1**, **AP3**, **AP4**, and **AP6** for HDAC6 and HDAC10. (A, B) Western blot analysis of HDAC6 and HDAC10 degradation in MM.1S cells treated for 24 h with **AP1**, **AP3**, **AP4**, and **AP6** at different concentrations. GAPDH was selected as loading control. Representative image of n = 2 biologically independent experiments, each performed in triplicates. (C, D) DC_{50} values were obtained by fitting D_{max} values to a variable slope response model (three parameters). Representative graph of n = 2 biologically independent experiments, each performed in triplicates. For mean ± SD see **Table 2**.

Cell viability assays

As both HDAC6 and HDAC10 are involved in the pathogenesis of cancer, but since single treatment with either selective HDAC6 or HDAC10 inhibitors evoke only low to moderate effects on cell viability[34-36], we aimed to investigate the potential antiproliferative effects of dual HDAC6/10 degraders. Consequently, we tested **AP1-AP6** in viability assays against the multiple myeloma cell line MM.1S as well as the breast cancer cell line MCF-7. Both cell lines were chosen because they are commonly used

to characterize HDAC6 degraders[8, 10, 12]. Interestingly, all compounds showed low or no inhibition of cell viability (**Table S1, Figure S1**, Supplementary Information). To rule out that the limited antiproliferative effects in MCF-7 cells comes from absence of degradation, we treated MCF-7 cells for 24 h with 1 or 5 μM of **AP1-AP6** and analyzed the HDAC6 and HDAC10 levels by immunoblot analysis (**Figure S2**, Supplementary Information). Consistent with the results obtained in MM.1S cells, **AP1**, **AP3**, and **AP6** were identified as potent degraders of HDAC6 and HDAC10, while **AP2** and **AP5** were less effective. Again, the phenylglutarimides **AP4** and **AP6** showed a pronounced "hook effect" at 5 μM.

AP1, a Tubastatin A and pomalidomide-based degrader, induced selective degradation of class IIb HDACs

Next, we continued our assessment of degradation in multiple myeloma MM1.S cells. To better understand these class IIb HDAC degraders, we further conducted degradation selectivity studies to investigate their abilities to degrade other subtypes of HDACs. Here, we chose the isoforms of HDAC1 and HDAC8 from class I and HDAC4 from class IIa. For **AP3** and **AP6**, which contain the bicyclic derivative-based warhead, both PROTACs showed a trend toward degrading HDAC1, HDAC4, and HDAC8 compared to the vehicle control group (**Figure 5A**). In contrast, the Tubastatin A-based degrader **AP4** caused no relevant HDAC1 or HDAC4 degradation and only slight HDAC8 degradation, while **AP1** induced no off-target degradation at all (**Figure 5B**).

To validate functional effects on enzymatic activity of degraders in cells levels in cells, the acetylation levels of HDAC substrate proteins like Ac-α-tubulin and Ac-histone H3 were investigated by immunoblot analysis for **AP1**, **AP3**, **AP4**, and **AP6** using Vorinostat (SAHA) as a positive control. All compounds caused an upregulation of Ac-α-tubulin, a known substrate of HDAC6, thereby indicating an

inhibition of HDAC6 activity. The pomalidomide-based degraders **AP1** and **AP6** induced upregulation of Ac-alpha-tubulin comparable to that of vorinostat. This effect is even more substantial in the case of phenylglutarimide-based PROTACs **AP4** and **AP6**, with **AP4**. These results are consistent with the corresponding DC_{50} values of the HDAC6 degradation. In contrast, no PROTAC upregulated Ac-histone H3 levels, a substrate of HDAC1-3, while treatment with the positive control Vorinostat resulted in strong hyperacetylation of histone H3. Taken together, these results identify **AP1** as a potent and highly selective class IIb HDAC degrader. **AP1** spares HDAC1, 4, and 8, and does not cause histone H3 hyperacetylation, confirming the absence of class I HDAC inhibition or degradation. Therefore, and due to the absence of a "hook effect", we chose to focus on **AP1** for subsequent mode of action studies.

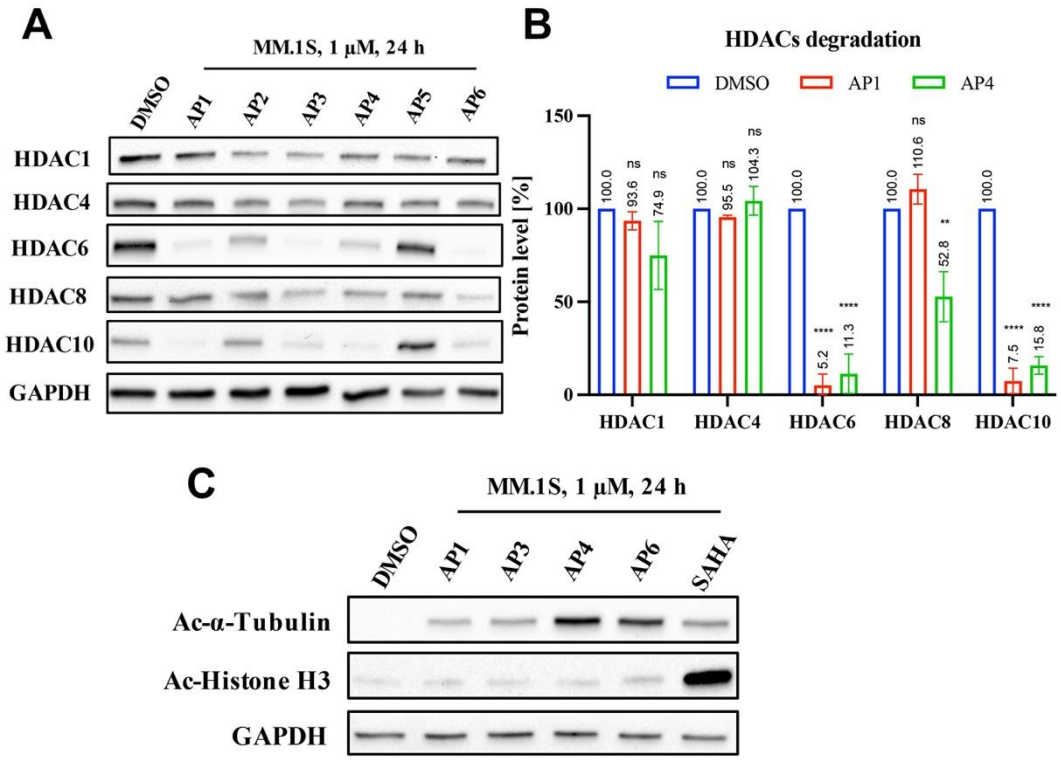

Figure 5. Degradation selectivity of **AP1**, **AP3**, **AP4**, and **AP6**. (A) MM.1S cells were treated with 1 μM of the respective PROTAC for 24 h. HDAC1, 4, 6, 8, and 10 levels were detected by western blot.

GAPDH was chosen as loading control. Representative image of n = 3 replicates. (B) Densitometric analysis of HDAC1, 4, 6, 8, and 10 levels after treatment with **AP1** and **AP4.** Data from n = 3 replicates. Statistical analysis was performed by using one-way ANOVA in GraphPad Prism 8. Statistical significance was indicated with asterisks (ns = no significance; ** = $p < 0.01$; **** = $p < 0.0001$). (C) Representative immunoblot analysis of acetylated α-tubulin and histone H3. MM.1S cells were incubated for 24 h at a concentration of 1 μM. Afterward, cell lysates were immunoblotted with an anti-acetyl-α-tubulin and anti-acetyl-histone H3 antibody. Vorinostat (SAHA) was used as positive control, and GAPDH was chosen as loading control. Representative image of n = 2 biologically independent experiments, each performed in triplicates.

AP1 degrades class IIb HDACs via the ubiquitin-proteasome system

To confirm the ubiquitin-proteasome system's (UPS) involvement in the degradation of HDAC6 and HDAC10, we conducted rescue experiments using binding competitors and an UPS inhibitor. In addition, we synthesized a non-degrading control **AP1-N**, which contains a methylated glutarimide ring (**Scheme S1**, Supplementary Information), and thus cannot bind to CRBN. Since pretreatment with competitors can increase cytotoxicity, we reduced the treatment time to 6 h. Initial experiments without cotreatments confirmed that the reduced treatment time is not affecting the degradation of class IIb HDACs by our PROTACs (**Figure 6A**). In the subsequent mode of action studies, we pretreated MM.1S cells for 0.5 h with 10 μM of the binding competitors Tubastatin A, Pomalidomide and the NEDD8-activating enzyme inhibitor MLN4924. Afterward, the cells were treated for 6 h with **AP1** (1 μM). The results are summarized in **Figure 6B.** Only the treatment with **AP1** alone induced significant degradation of HDAC6 and HDAC10, whereas **AP1-N** could not reduce the protein levels of either isoform. HDAC6

and HDAC10 levels were recovered for the groups with pretreatments, thereby confirming that **AP1** induces class IIb HDAC degradation *via* binding to CRBN and HDACs and leading to neddylation-dependent degradation.

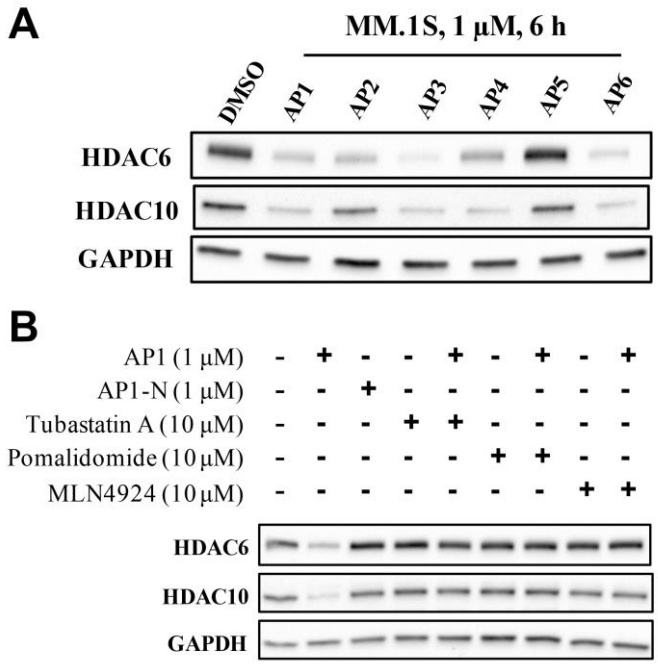

Figure 6. Rescue experiments with degrader **AP1**. (A) MM.1S cells were treated with 1 μM of the respective PROTAC for 6 h. HDAC6 and 10 levels were detected by western blot. DMSO served as vehicle control and GAPDH was chosen as loading control. Representative image of n = 3 replicates. (B) Pretreatments of MM.1S cells for 30 min were carried out in the co-treatment groups containing the tubastastin A (10 μM), pomalidomide (10 μM), MLN4924 (10 μM), and then treated for 6 h with 1 μM of **AP1**. GAPDH was chosen as loading control. **AP1** served as positive and **AP1-N** as negative control. Representative image of n = 2 biologically independent experiments, each performed in triplicates.

Quantitative proteomics

In order to analyze the selectivity profile of **AP1** by an orthogonal method, we performed quantitative proteomics analysis. To this end, MM.1S cells were treated for 6 h with 1 μM of **AP1**, tubastatin A, and

vehicle control (DMSO) and subsequently subjected to MS-based whole proteome analysis. Despite the unreliable detection of HDAC6 and HDAC10, likely due to low protein expression levels, we successfully monitored the protein levels of HDAC1-3 and HDAC7. None of the detected HDACs were significantly downregulated, confirming **AP1**'s excellent selectivity toward HDAC6 and HDAC10 (**Figure S3**, Supplementary Information).

To further investigate the proteome-wide degradation specificity of **AP1**, we performed quantitative proteomics analysis in MOLT4 cells. In this experiment, HDAC6, but not HDAC10, could be quantified. Among the identified HDACs (HDAC1-4 and HDAC6-8), **AP1** selectively degraded HDAC6 after 5 hours of incubation with 1 μM of **AP1** (**Figure 7**). In addition, degradation of the pomalidomide neosubstrates IKZF1 and ZFP1 was observed. In conclusion, MS-based whole proteome analysis in combination with our western blot results verified that **AP1** is a selective degrader of HDAC6/10.

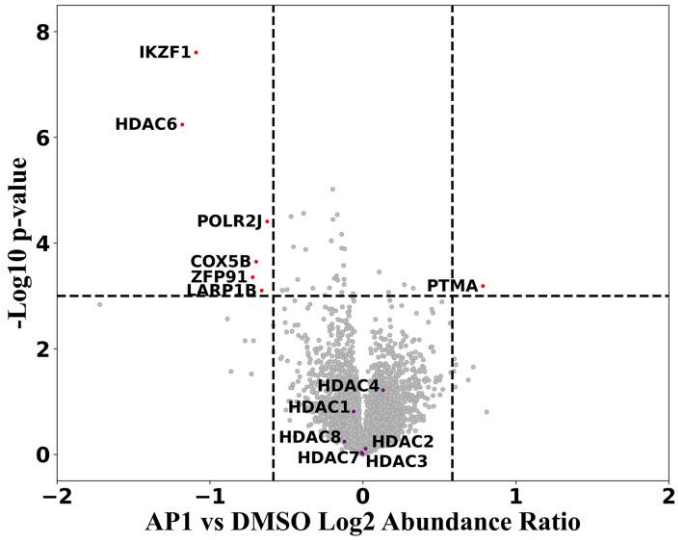

Figure 7. Quantitative proteomics of MOLT-4 cell lysates after treatment with **AP1** (1 μM) for 5 hours. Hits are labelled in red dots with the thresholds: Fold change > 1.5 and P value < 0.001. Other HDAC subtypes are labelled in purple dots.

Ternary complex modeling

The formation of ternary complexes has been identified as a primary mechanism driving PROTAC-induced degradation[22]. In recent years, several crystal structures elucidating such ternary complexes have been resolved[37, 38]. To gain deeper insights into the binding mechanisms of **AP1**-induced ternary complexes, modeling studies focusing on HDAC6-AP1-CRBN and HDAC10-AP1-CRBN complexes were conducted. Crystal structures of HDAC6 (PDB ID: 6THV), HDAC10 (PDB ID: 6WBQ), and cereblon (PDB ID: 8OIZ) were selected as templates. Despite the non-human origin of the chosen HDAC6 and HDAC10 structures, the presence of Tubastatin A as the co-crystallized ligand within their respective pockets is expected to enhance the accuracy of the modeling outcomes. An established protocol, method 4B[39, 40], was employed for generating the ternary complexes (see Experimental section for details). As a result (**Figure 8**), degrader **AP1** exhibited favorable interactions with the POI and CRBN in both cases.

In the top pose of the modelled HDAC10-AP1-CRBN complex (**Figure 8**), the Tubastatin A-based warhead is prominently engaged in metal chelation with the Zn^{2+} within the HDAC10 pocket, while also forming hydrogen bonds with residues H136, D267, and Y307. Simultaneously, the pomalidomide-based E3 ligand formed a crucial hydrogen bond with residue H378 within the CRBN pocket. Additionally, interactions of both S203 and W400 with the amide on the linker are observed. In the case of HDAC6-AP1-CRBN, similar interactions are predicted. The HDAC warhead of **AP1** is observed to form metal chelation with the Zn^{2+} and hydrogen bonds with H574 and D612 inside the HDAC6 catalytic pocket. In addition to the key hydrogen bond formed with H378, the pomalidomide-based E3 ligand also forms

hydrogen bonds with N351, E377, and S379 within CRBN. These interactions likely contribute to the enhanced degradation potency of **AP1** towards HDAC6 compared to HDAC10.

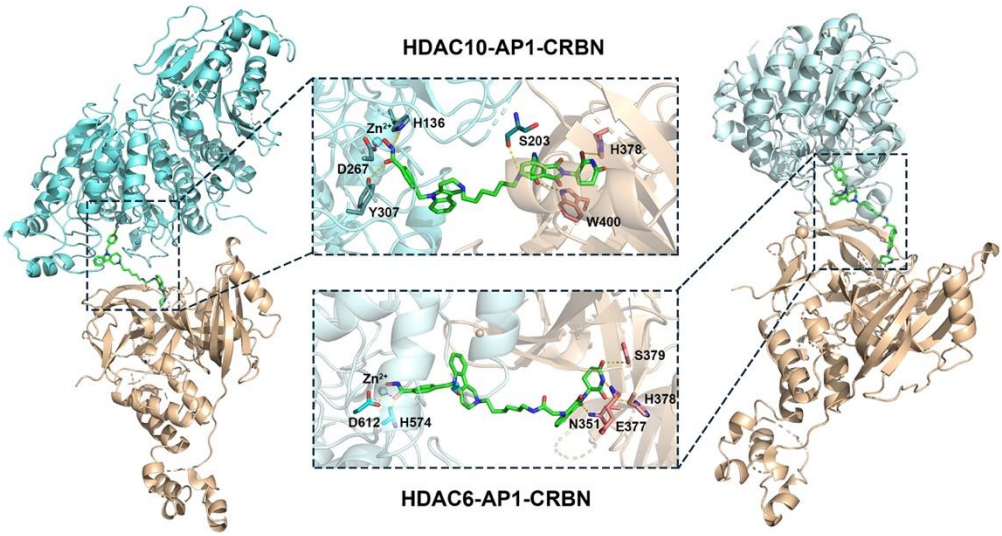

Figure 8. Ternary complex modeling of HDAC6-AP1-CRBN and HDAC10-AP1-CRBN. Hydrogen bonds are shown as yellow dashes and metal chelation is indicated as purple dashes. Ternary complex poses are derived from Method 4B in the MOE software. The binding modes were predicted with the ligand interaction moiety and the figures were prepared with PyMOL.

CONCLUSIONS

In conclusion, our work demonstrates the successful design, synthesis, and biological evaluation of first-in-class selective degraders for the class IIb HDACs 6 and 10. Utilizing the dual HDAC6/10 inhibitor Tubastatin A and a ring-opened analog, we connected these molecules to pomalidomide and a phenylglutarimide derivative *via* established PROTAC linkers to act as cereblon recruiters. This approach led to the discovery of **AP1**, a potent degrader of class IIb HDACs (HDAC6 DC_{50} = 13 nM; HDAC10 DC_{50} = 29 nM). Importantly, **AP1** showed no significant degradation of HDAC1/8 (class I) and HDAC4 (class IIa), nor did it induce histone H3 hyperacetylation, confirming its selectivity for class

IIb HDACs. Furthermore, **AP1** exhibited low cytotoxicity against hematological and solid cancer cell lines, making it a valuable tool compound for the chemical knockdown of class IIb HDACs.

EXPERIMENTAL SECTION

chemistry

General information. Chemicals were obtained from abcr GmbH, Acros Organics, Carbolution Chemicals, Fluorochem, Sigma-Aldrich, TCI Chemicals, BLDpharm or VWR and used without further purification. Technical grade solvents were distilled prior to use. For all HPLC purposes, acetonitrile in HPLC-grade quality (HiPerSolv CHROMANORM, *VWR*) was used. Water was purified with a PURELAB flex® (*ELGA VEOLIA*). Air-sensitive reactions were carried out under argon atmosphere utilizing standard *Schlenk* techniques. If no solvent is stated an aqueous solution was prepared with demineralized water. Mixtures of two or more solvents are specified as "solvent A"/"solvent B", 3/1, *v*/*v*; meaning that 100 mL of the respective mixture consists of 75 mL of "solvent A" and 25 mL of "solvent B". **Thin-layer chromatography (TLC)** was carried out on prefabricated plates (silica gel 60, F_{254}, *Merck*). Components were visualized either by irradiation with ultraviolet light (254 nm or 366 nm) or by staining appropriately. **Column Chromatography:** If not stated otherwise, column chromatography was carried out on silica gel (60 Å, 40-60 µm, *Acros Organics*). In addition, a flash column system (puriFlash® XS 520 Plus, Advion Interchim Scientific) was utilized for the purification of the synthesized compounds. **Nuclear Magnetic Resonance Spectroscopy (NMR):** Proton (^{1}H) and carbon (^{13}C) NMR spectra were recorded either on a *Bruker* AVANCE 500 MHz at a frequency of 500 MHz (^{1}H) and 126 MHz (^{13}C) or on a *Bruker* AVANCE III HD 600 MHz at a frequency of 600 MHz (^{1}H) and 151 MHz (^{13}C). The chemical shifts are given in parts per million (ppm). As solvents deuterated chloroform ($CDCl_3$)

and deuterated dimethyl sulfoxide (DMSO-d_6) were used. The residual solvent signal ($CDCl_3$: ^{1}H NMR: 7.26 ppm, ^{13}C NMR: 77.1 ppm; DMSO-d_6: ^{1}H NMR: 2.50 ppm, ^{13}C NMR: 39.52 ppm) was used for calibration. The multiplicity of each signal is reported as singulet (s), doublet (d), triplet (t), quartet (q), pentet (p), sextet (sext), multiplet (m) or combinations thereof. Multiplicities and coupling constants are reported as measured and might disagree with the expected values. **Mass Spectrometry:** High resolution electrospray ionization mass spectra (HRMS-ESI) were acquired with *Bruker Daltonik GmbH* micrOTOF coupled to a an *LC Packings* Ultimate HPLC system and controlled by micrOTOFControl3.4 and HyStar 3.2-LC/MS, with a *BrukerDaltonik GmbH* ESI-qTOF Impact II coupled to a *Dionex* UltiMateTM 3000 UHPLC system and controlled by micrOTOFControl 4.0 and HyStar 3.2-LC/MS or with a micrOTOF-Q mass spectrometer (*Bruker*) with ESI-source coupled with an HPLC Dionex UltiMate 3000 (*Thermo Scientific*). Low resolution electrospray ionisation mass spectra (LRMS-ESI) were acquired with an *Advion* expression® compact mass spectrometer (CMS) coupled with an automated TLC plate reader Plate Express® (*Advion*). **High Performance Liquid Chromatography (HPLC)**: A *Thermo Fisher Scientific* UltiMate^{TM} 3000 UHPLC system with a Nucleodur 100-5 C18 (250 x 4.6 mm, *Macherey Nagel*) with a flow rate of 1 mL/min and a temperature of 25 °C or a 100-5 C18 (100 x 3 mm, *Macherey Nagel*) with a flow rate of 0.5 mL/min and a temperature of 25 °C with an appropriate gradient were used. For preparative purposes a AZURA Prep. 500/1000 gradient system (*Knauer*) with a Nucleodur 110-5 C18 HTec (150 x 32 mm, *Macherey Nagel*) column with 20 mL/min was used. Detection was implemented by UV absorption measurement at a wavelength of λ = 220 nm and λ = 250 nm. Bidest. H_2O (A) and ACN (B) were used as eluents with an addition of 0.1% TFA for eluent A. **Purity:** The purity of all final compounds was 95% or higher. Purity was determined via HPLC with the Nucleodur 100-5 C18 (250 x 4.6 mm, *Macherey Nagel*) at 250 nm. After column equilibration

for 5 min, a linear gradient from 5% A to 95% B in 5 min followed by an isocratic regime of 95% B for 12 min was used.

General procedures

General procedure A for the synthesis of compound 16-17 and 20-21

To a solution of compound **11** or **14** (1.0-1.1 eq.) in anhydrous DMF (3 mL), HATU (2 eq.) and DIPEA (3 eq.) were added. The mixture was stirred at room temperature for 0.5 h. Afterwards, a solution of Boc-deprotected compound **4** or **9** (1 eq) in anhydrous DMF (2 mL) was added and the reaction mixture was then stirred for 17 h at room temperature. The mixture was poured into water (100 mL) and extracted with ethyl acetate (3 x 30 mL). The combined organic layer was then washed with water (3 x 50 mL) and followed by brine (50 mL), dried over anhydrous Na_2SO_4, filtered, and concentrated *in vacuo* to yield the crude products, which were subsequently purified by silica column chromatography.

General procedure B for the synthesis of compound 18-19

To a solution of compound **12** or **15** (1 eq.) in DMF/H_2O (5 mL: 0.5 mL), compound **5** (1.05 eq.), ascorbic acid (3 eq.), and $CuSO_4$ (1 eq.) were added. The mixture was stirred at room temperature for 2-4 h. Next, the mixture was poured into water (100 mL) and extracted with ethyl acetate (3 x 30 mL). The combined organic layer was then washed with water (3 x 50 mL)and followed by brine (50 mL), dried over anhydrous Na_2SO_4, filtered, and concentrated *in vacuo* to provide the crude products, which were then purified by flash column chromatography (0→10% MeOH in EtOAc, 0-10 min; 10% MeOH in EtOAc,10-30 min).

General procedure C for the synthesis of compounds AP1-AP6

To a solution of compound **16-21** (1 eq.) in methanol/ethanol (10 mL), Pd/C (5% palladium on carbon, 0.05 eq.) was added. The flask was evacuated and flushed with H_2 and the mixture was stirred at room temperature under H_2 atmosphere overnight. The completion of the reaction was monitored by HPLC and additional Pd $(OH)_2$/C (0.05 eq.) was added into the system if the conversion was not complete[41]. The resulting reaction solution was filtered over Celite® and the solvents removed under reduced pressure. The subsequent purification was carried out utilizing reverse phase flash column chromatography (0→100% ACN in water, 0-30 min).

Compound characterization

*Synthesis of tert-butyl 1,3,4,5-tetrahydro-2H-pyrido[4,3-b] indole-2-carboxylate (**1**)*

To a solution of phenylhydrazine hydrochloride (10.0 g, 69.2 mmol, 1 eq.) and *tert*-butyl 4-oxopiperidine-1-carboxylate (15.2 g, 76.1 mmol, 1.1 eq.) in toluene (150 mL), 2,4,6-tripropyl-1,3,5,2,4,6-trioxatriphosphinane 2,4,6-trioxide (11.0 ml, 17.3 mmol, 0.25 eq., 50 % solution in EtOAc) was added as the catalyst. The mixture was stirred at 90 °C for 16 h. The completion of the reaction was monitored by TLC. The solvent was removed *in vacuo*. The crude product was then dissolved in a mixture of ethyl acetate (100 mL) and water (100 mL). The extraction was performed with the ethyl acetate (3 x 100 mL) and the combined organic layer was washed with brine and dried over anhydrous Na_2SO_4. The filtrate was concentrated *in vacuo* to afford the crude product, which was then purified by silica column (CyH/EtOAc 2:1, *v/v*) to yield compound **1** (11.3 g, 60%). **^{1}H NMR** (500 MHz, $CDCl_3$) δ 7.92 (s, 1H), 7.45 (dd, *J* = 7.7, 1.3 Hz, 1H), 7.34 – 7.29 (m, 1H), 7.16 (ddd, *J* = 8.1, 7.1, 1.3 Hz, 1H), 7.10 (td, *J* = 7.4, 1.1 Hz, 1H), 4.65 (s, 2H), 3.82 (t, *J* = 5.7 Hz, 2H), 2.88 – 2.79 (m, 2H), 1.51 (s, 9H).

^{13}C NMR (126 MHz, $CDCl_3$) δ 155.4, 136.0, 132.1, 125.8, 121.8, 119.7, 117.8, 110.8, 107.8, 80.0, 41.3, 28.6, 28.5, 23.7. **LC-MS (ESI)**, $[M-H]^-$ *m/z*: 271.1.

*Synthesis of tert-butyl 5-(4-(methoxycarbonyl)benzyl)-1,3,4,5-tetrahydro-2H-pyrido[4,3-b]indole-2-carboxylate (**2**)*

To a solution of compound **1** (4.00 g, 14.7 mmol, 1 eq.) in acetonitrile (100 mL), methyl 4-(bromomethyl)benzoate (3.53 g, 15.4 mmol, 1.05 eq.) and Cs_2CO_3 (9.57 g, 29.4 mmol, 2 eq.) were added. The mixture was stirred and refluxed for 15 h. The completion of the reaction was monitored by TLC. The solvent was removed *in vacuo.* The crude product was then dissolved in a mixture of ethyl acetate (75 mL) and water (75 mL). The extraction was performed with the ethyl acetate (3 x 50 mL) and the combined organic layer was washed with brine (50 mL) and dried over anhydrous Na_2SO_4. The filtrate was concentrated *in vacuo* to afford the crude product, which was then purified by silica column (CyH/EtOAc 4:1, *v/v*) to afford compound **2** (3.51 g, 57%). **^{1}H NMR** (500 MHz, $CDCl_3$) δ 7.97 – 7.91 (m, 2H), 7.54 – 7.48 (m, 1H), 7.19 (dt, *J* = 8.1, 1.0 Hz, 1H), 7.14 (dtd, *J* = 14.0, 6.9, 1.4 Hz, 2H), 7.08 – 7.03 (m, 2H), 5.30 (s, 2H), 4.69 (s, 2H), 3.89 (s, 3H), 3.81 (t, *J* = 5.7 Hz, 2H), 2.70 (t, *J* = 5.5 Hz, 2H), 1.50 (s, 9H). **^{13}C NMR** (126 MHz, $CDCl_3$) δ 166.8, 155.3, 143.0, 136.9, 133.6, 130.3, 129.6, 126.2, 125.6, 121.8, 119.8, 118.0, 109.3, 108.0, 80.1, 52.3, 46.4, 41.3, 28.6, 27.1, 22.7. **LC-MS (ESI)**, $[M+H]^+$ *m/z*: 421.3.

*Synthesis of tert-butyl 5-(4-((benzyloxy)carbamoyl)benzyl)-1,3,4,5-tetrahydro-2H-pyrido[4,3-b]indole-2-carboxylate (**3**)*

To a solution of compound **2** (3.00 g, 7.14 mmol, 1 eq.) in THF/MeOH/H_2O (60 mL/12 mL/12 mL), $LiOH \cdot H_2O$ (0.784 g, 17.8 mmol, 2.5 eq.) was added. The mixture was stirred at room temperature for about 17 h. Heating at 50 °C for extra 1-2 h was performed when the reaction was not complete. Upon the completion of the hydrolysis, the solvents were removed *in vacuo*. The crude product was dissolved with water (50 mL) and acidified with HCl (0.5 M in water) until no more precipitate was formed. The resulting precipitate was collected *via* filtration, washed with water and dried *in vacuo* for the next step without further purification. To a solution of the dried precipitate (2.81 g, 6.91 mmol, 1 eq.) in anhydrous DMF (60 mL), HATU (5.26 g, 13.8 mmol, 2 eq.) and DIPEA (2.68 g, 20.7 mmol, 3 eq.) were added. The mixture was stirred for 30 min at room temperature. Afterwards, *O*-benzylhydroxylamine hydrochloride (2.21 g, 13.8 mmol, 2 eq.) was added and the reaction mixture was stirred for 16 h. The completion of the reaction was monitored by TLC. The mixture was poured into water (150 mL) and extracted with ethyl acetate (3 x 50 mL). The combined organic layer was then washed with water (3 x 50 mL) and followed by brine (50 mL), dried over anhydrous Na_2SO_4, filtered, and concentrated *in vacuo* to afford the crude product, which was then purified by flash column chromatography (0→50% EtOAc in CyH, 0-10 min; 50% EtOAc in CyH, 10-35 min) to generate compound **3** (2.67 g, 75%). **^{1}H NMR** (600 MHz, $CDCl_3$) δ 8.59 (s, 1H), 7.56 (d, *J* = 7.9 Hz, 2H), 7.49 (d, *J* = 7.3 Hz, 1H), 7.41 (dd, *J* = 7.3, 2.2 Hz, 2H), 7.38 – 7.33 (m, 3H), 7.19 – 7.09 (m, 3H), 7.00 (d, *J* = 8.0 Hz, 2H), 5.26 (s, 2H), 5.00 (s, 2H), 4.67 (s, 2H), 3.79 (t, *J* = 5.8 Hz, 2H), 2.67 (t, *J* = 5.7 Hz, 2H), 1.49 (s, 9H). **^{13}C NMR** (151 MHz, $CDCl_3$) δ 166.0, 155.3, 142.1, 136.8, 135.4, 134.1, 131.2, 129.4, 129.0, 128.8, 127.7, 126.5, 125.5, 121.8, 119.8, 118.0, 109.3, 107.9, 80.1, 78.5, 46.2, 41.6, 40.8, 28.6, 22.6. **LC-MS (ESI)**, $[M-H]^-$ m/z: 510.4.

*Synthesis of tert-butyl (6-(5-(4-((benzyloxy)carbamoyl)benzyl)-1,3,4,5-tetrahydro-2H-pyrido[4,3-b]indol-2-yl)hexyl)carbamate (**4**)*

To a solution of compound **3** (1.46 g, 2.86 mmol, 1 eq.) in DCM (20 mL), TFA (4 mL) was added. The mixture was stirred at room temperature for 2 h and the complete removal of *tert*-butyl group was monitored by HPLC. Afterwards, the mixture was dried *in vacuo* to offer the crude product for the next step. To a solution of the resulting crude product in anhydrous DMF (50 mL), *tert*-butyl (6-bromohexyl)carbamate (1.20 g, 4.29 mmol, 1.5 eq.) and K_2CO_3 (0.790 g, 5.72 mmol, 2 eq.) were added. The mixture was stirred at room temperature for 18 h. The completion of the reaction was monitored by HPLC. The mixture was poured into water (150 mL) and extracted with ethyl acetate (3 x 50 mL). The combined organic layer was then washed with water (3 x 50 mL) and followed by brine (50 mL), dried over anhydrous Na_2SO_4, filtered, and concentrated *in vacuo* to yield the crude product, which was then purified by silica column chromatography (EtOAc: MeOH 10:1, *v/v*) to yield compound **4** (1.16 g, 66%). **^{1}H NMR** (600 MHz, $CDCl_3$) δ 7.54 (d, *J* = 8.0 Hz, 2H), 7.41 (ddd, *J* = 14.4, 7.2, 1.9 Hz, 3H), 7.37 – 7.31 (m, 3H), 7.16 – 7.06 (m, 3H), 6.96 (d, *J* = 8.1 Hz, 2H), 5.23 (s, 2H), 4.98 (s, 2H), 3.85 (s, 2H), 3.09 (q, *J* = 6.8 Hz, 2H), 2.99 – 2.91 (m, 2H), 2.76 (d, *J* = 5.8 Hz, 2H), 2.68 (t, *J* = 7.9 Hz, 2H), 1.69-1.64 (m, 2H), 1.50 – 1.48-1.46 (m, 2H), 1.43 (s, 9H), 1.36-1.33 (m, 4H). **^{13}C NMR** (151 MHz, $CDCl_3$) δ 165. 8, 156.2, 141. 9, 136.9, 135.5, 133.1, 131.2, 129.4, 128.9, 128.9, 128.7, 128.6, 127.8, 126.5, 125.9, 121.6, 119.7, 117.9, 109.3, 107.5, 79.2, 78.3, 57.5, 50.5, 49.5, 46.3, 40.6, 30.1, 28.6, 27.2, 26.8, 26.7, 22.2. **LC-MS (ESI)**, $[M+H]^+$ *m/z*: 611.4.

*Synthesis of 4-((2-(6-azidohexyl)-1,2,3,4-tetrahydro-5H-pyrido[4,3-b]indol-5-yl)methyl)-N-(benzyloxy)benzamide (**5**)*

To a solution of compound **3** (0.850 g, 1.66 mmol, 1 eq.) in DCM (20 mL), TFA (4 mL) was added. The mixture was stirred at room temperature for 2 h and the complete removal of *tert*-butyl group was monitored by HPLC. Afterwards, the mixture was dried *in vacuo* to provide the crude product for the next step. To a solution of the resulting crude product in anhydrous DMF (30 mL), 1-azido-6-bromohexane (0.514 g, 2.49 mmol, 1.5 eq.) and K_2CO_3 (0.459 g, 3.32 mmol, 2 eq.) were added. The mixture was stirred at room temperature for 20 h. The completion of the reaction was monitored by HPLC. The mixture was poured into water (150 mL) and extracted with ethyl acetate (3 x 50 mL). The combined organic layer was then washed with water (3 x 50 mL) and followed by brine (50 mL), dried over anhydrous Na_2SO_4, filtered, and concentrated *in vacuo* to afford the crude product, which was then purified by flash column chromatography (0-10% MeOH in DCM, 0-10 min; 10% MeOH in DCM, 10-35 min) to provide compound **5** (0.634 g, 71%). Synthesis of 1-azido-6-bromohexane followed previously reported methods[42]. **^{1}H NMR** (600 MHz, $CDCl_3$) δ 8.99 (s, 1H), 7.54 (d, *J* = 8.0 Hz, 2H), 7.41 (ddd, *J* = 18.9, 7.0, 2.0 Hz, 3H), 7.38 – 7.32 (m, 3H), 7.15 – 7.06 (m, 3H), 6.98 (d, *J* = 8.0 Hz, 2H), 5.23 (s, 2H), 4.98 (s, 2H), 3.79 (s, 2H), 3.27 (t, *J* = 6.9 Hz, 2H), 2.89 (d, *J* = 5.8 Hz, 2H), 2.74 (d, *J* = 5.7 Hz, 2H), 2.65 (t, *J* = 7.8 Hz, 2H), 1.67 (q, *J* = 7.6 Hz, 2H), 1.62 (p, *J* = 7.1 Hz, 2H), 1.46 – 1.37 (m, 4H). **^{13}C NMR** (151 MHz, $CDCl_3$) δ 165.6, 142.0, 136.9, 135.5, 133.4, 131.2, 129.4, 129.4, 128.9, 128.8, 128.7, 128.6, 127.7, 126.6, 126.0, 121.4, 119.6, 117. 9, 109.2, 108.2, 78.3, 57.9, 51.5, 50.7, 49.7, 46.3, 28.9, 27.2, 27.2, 26.8, 22.6. **LC-MS (ESI)**, $[M+H]^+$ *m/z*: 537.5.

*Synthesis of methyl 4-((3-formyl-1H-indol-1-yl)methyl)benzoate (**6**)*

To a solution of 1*H*-indole-3-carbaldehyde (3.00 g, 20.7 mmol, 1 eq.) in acetonitrile (50 mL), methyl 4-(bromomethyl)benzoate (4.97 g, 21.7 mmol, 1.05 eq.) was added. The mixture was stirred and refluxed

for 15 h. The solvent was removed *in vacuo*. The crude product was then dissolved by a mixture of ethyl acetate (75 mL) and water (75 mL). The subsequent extraction was performed with the ethyl acetate (3 x 50 mL) and the combined organic layer was washed with brine (50 mL) and dried over Na_2SO_4. The filtrate was concentrated *in vacuo* to provide the crude, which was then purified by silica column chromatography (DCM: MeOH 50:1, *v/v*) to yield compound **6** (5.98 g, 99%). **^{1}H NMR** (600 MHz, $CDCl_3$) δ 10.02 (s, 1H), 8.34 (dt, *J* = 7.8, 1.2 Hz, 1H), 8.04 – 7.98 (m, 2H), 7.75 (s, 1H), 7.34-7.28 (m, 2H), 7.27 – 7.25 (m, 1H), 7.22 (d, *J* = 8.1 Hz, 2H), 5.43 (s, 2H), 3.90 (s, 3H). **^{13}C NMR** (151 MHz, $CDCl_3$) δ 184.8, 166. 6, 140.5, 138.6, 137.5, 130.5, 130.4, 127.0, 125.6, 124.5, 123.4, 122.4, 118.9, 110.4, 52.4, 50.8. **LC-MS (ESI)**, $[M+H]^+$ *m/z*: 294.1.

*Synthesis of methyl 4-((3-((methylamino)methyl)-1H-indol-1-yl)methyl)benzoate (**7**)*

To a solution of compound **6** (4.00 g, 13.6 mmol, 1 eq.) in MeOH and DCM (100 mL: 10 mL), methylamine (2.09 mL, 20.5 mmol, 1.5 eq., 9.8 M in MeOH) was added. The mixture was stirred at room temperature for 19 h. The complete consumption of the starting material was monitored by HPLC. Afterwards, the mixture was cooled in ice bath and $NaBH_4$ (1.03 g, 27.3 mmol, 2 eq.) was added slowly. The reaction mixture was then stirred for another 3 h. The completion of the reaction was monitored by HPLC. The resulting mixture was filtered and the filtrate was then concentrated *in vacuo* to provide the crude product (3.66 g, 87%) which was used without further purification. **^{1}H NMR** (600 MHz, $CDCl_3$) δ 7.97 – 7.92 (m, 2H), 7.68 (dd, *J* = 7.1, 1.6 Hz, 1H), 7.22 (s, 1H), 7.20 – 7.20-7.17 (m, 2H), 7.15-7.13 (m, 3H), 5.32 (s, 2H), 4.03 (s, 2H), 3.88 (s, 3H), 2.50 (s, 3H). **^{13}C NMR** (151 MHz, $CDCl_3$) δ 166.8, 142.6, 136.6, 130.2, 129.7, 128.0, 127.9, 126.8, 122.4, 120.0, 119.1, 111.7, 109.9, 52.3, 50.0, 45.6, 34.8. **LC-MS (ESI)**, $[M-H]^-$ *m/z*: 307.3.

*Synthesis of methyl 4-((3-(((6-((tert-butoxycarbonyl)amino)hexyl)(methyl)amino)methyl)-1H-indol-1-yl)methyl)benzoate (**8**)*

To a solution of compound **7** (2.79 g, 9.05 mmol, 1 eq.) in anhydrous DMF (60 mL), *tert*-butyl (6-bromohexyl)carbamate (3.80 g, 13.6 mmol, 1.5 eq.) and K_2CO_3 (2.50 g, 18.1 mmol, 2 eq.) were added. The mixture was stirred at room temperature for 15 h. The completion of the reaction was monitored by HPLC. The mixture was poured into water (150 mL) and extracted with ethyl acetate (3 x 50 mL). The combined organic layer was then washed with water (3 x 50 mL)and followed by brine (50 mL), dried over anhydrous Na_2SO_4, filtered, and concentrated *in vacuo* to provide the crude product, which was then purified by silica column (DCM: MeOH 50:1, *v/v*, 1% Et_3N) to afford compound **8** (3.08 g, 67%). **^{1}H NMR** (600 MHz, DMSO-d_6) δ 7.91 – 7.86 (m, 2H), 7.63 (d, *J* = 7.8 Hz, 1H), 7.39 – 7.32 (m, 2H), 7.29 – 7.23 (m, 2H), 7.07 (ddd, *J* = 8.2, 7.0, 1.2 Hz, 1H), 7.03 – 6.98 (m, 1H), 6.75 – 6.67 (m, 1H), 5.48 (s, 2H), 3.81 (s, 3H), 3.61 (s, 2H), 2.87 (q, *J* = 7.2, 6.7 Hz, 2H), 2.34 (t, *J* = 7.3 Hz, 2H), 2.12 (s, 3H), 1.46 (dq, *J* = 14.6, 7.4, 6.9 Hz, 2H), 1.36 (s, 9H), 1.34 (t, *J* = 6.7 Hz, 2H), 1.28 – 1.19 (m, 4H). **^{13}C NMR** (151 MHz, DMSO-d_6) δ 165.9, 155.5, 143.9, 136.2, 129.4, 128.6, 128.2, 127.0, 121.3, 119.5, 118.8, 111.8, 109.9, 77.2, 56.5, 54.9, 52.4, 52.0, 48.5, 41.7, 29.5, 28.2, 26.8, 26.6, 26.2. **LC-MS (ESI)**, $[M+H]^+$ *m/z*: 508.5.

*Synthesis of tert-butyl (6-(((1-(4-((benzyloxy)carbamoyl)benzyl)-1H-indol-3-yl)methyl)(methyl)amino)hexyl)carbamate (**9**)*

To a solution of compound **8** (3.08 g, 6.07 mmol, 1 eq.) in THF/MeOH/H2O (60 mL: 12 mL: 12 mL) was added $LiOH·H_2O$ (0.509 g, 12.1 mmol, 2 eq.), the mixture was stirred at room temperature for 16.5

h. Heating at 50 ℃ for extra 1-2 h was operated when the reaction was not complete. Upon the completion of the hydrolysis, the solvent was removed *in vacuo*. The crude was dissolved with water and acidified with HCl (0.5 M in water) until no more precipitate is formed, the resulting precipitate was collected *via* filtration, washed with water and dried *in vacuo* for the next step without further purification. To a solution of the dried precipitate (2.64 g, 5.35 mmol, 1 eq.) prepared in the last step in anhydrous DMF (60 mL) were added HATU (4.07 g, 10.7 mmol, 2 eq.) and DIPEA (2.07 g, 16.0 mmol, 3 eq.), the mixture was stirred for 30 min at room temperature, after which, O-benzylhydroxylamine hydrochloride (1.71 g, 10.7 mmol, 2 eq.) was added into the system and stirred 17 h. Completion of the reaction was monitored by TLC. The mixture was poured into water (150 mL) and extracted with ethyl acetate (3 x 50 mL). The combined organic layer was then washed with water (3 x 50 mL) and followed by brine(50 mL), dried over anhydrous Na_2SO_4, filtered and concentrated *in vacuo* to offer the crude, which was then purified by silica column (DCM: MeOH 50:1, *v/v*, 1% Et_3N) to offer the compound **9** (2.55 g, 80%). **^{1}H NMR** (600 MHz, $CDCl_3$) δ 7.68 (d, *J* = 7.7 Hz, 1H), 7.61 (d, *J* = 7.9 Hz, 2H), 7.42 (dd, *J* = 7.4, 2.0 Hz, 2H), 7.38 – 7.31 (m, 3H), 7.19 – 7.14 (m, 2H), 7.14 – 7.10 (m, 2H), 7.09 (d, *J* = 8.1 Hz, 2H), 5.30 (s, 2H), 5.01 (s, 2H), 3.74 (s, 2H), 2.96 (q, *J* = 6.9 Hz, 2H), 2.42 (t, *J* = 7.6 Hz, 2H), 2.28 (s, 3H), 1.53 (p, *J* = 7.3 Hz, 2H), 1.42 (s, 9H), 1.36 (p, *J* = 7.3 Hz, 2H), 1.26 (q, *J* = 7.3 Hz, 2H), 1.24 – 1.17 (m, 2H). **^{13}C NMR** (151 MHz, $CDCl_3$) δ 165.5, 156.2, 141.6, 136.5, 135.6, 131.5, 129.4, 129.4, 128.8, 128.7, 128.6, 128.1, 127.8, 127.0, 122.1, 119.7, 119.7, 109.7, 79.3, 78.3, 63.9, 56.6, 52.5, 49.8, 42.2, 40.6, 30.0, 28.6, 27.0, 26.5. **LC-MS (ESI)**, $[M+H]^+$ *m/z*: 599.6.

*Synthesis of hex-5-yn-1-yl (2-(2,6-dioxopiperidin-3-yl)-1,3-dioxoisoindolin-4-yl)glycinate (**12**)*

The *tert*-butyl (2-(2,6-dioxopiperidin-3-yl)-1,3-dioxoisoindolin-4-yl)glycinate (compound **10**, 1.36 g) was synthesized following the previously reported method[27]. To a solution of compound **10** (0.590 g, 1.52 mmol, 1 eq.) in DCM (15 mL) was added TFA (3 mL), the mixture was stirred at room temperature for 2 h, the complete removal of *tert*-butyl group was monitored by TLC, after which, the mixture was dried *in vacuo* to offer the crude, compound **11**, for the next step. To a solution of the resulting crude in anhydrous DMF (15 mL) were added HATU (1.16 g, 3.05 mmol, 2 eq.) and DIPEA (0.591 g, 4.57 mmol, 3 eq.), the mixture was stirred for 30 min at room temperature, after which, hex-5-yn-1-ol (0.299 g, 3.05 mmol, 2 eq.) was added into the system and stirred for 15 h. Completion of the reaction was monitored by HPLC. The mixture was poured into water (100 mL) and extracted with ethyl acetate (3 x 30 mL). The combined organic layer was then washed with water (3 x 50 mL) and followed by brine (50 mL), dried over anhydrous Na_2SO_4, filtered and concentrated *in vacuo* to offer the crude, which was then purified by silica column (CyH/EtOAc, 1:1, *v/v*) to offer the compound **12** (0.343 g, 55%).

^{1}H NMR (600 MHz, $CDCl_3$) δ 8.09 (s, 1H), 7.52 (dd, *J* = 8.5, 7.2 Hz, 1H), 7.17 (d, *J* = 7.2 Hz, 1H), 6.78 (d, *J* = 8.5 Hz, 1H), 6.70 (s, 1H), 4.93 (dd, *J* = 12.4, 5.4 Hz, 1H), 4.23 (t, *J* = 6.5 Hz, 2H), 4.07 (s, 2H), 2.93 – 2.86 (m, 1H), 2.86 – 2.70 (m, 2H), 2.23 (td, *J* = 7.0, 2.6 Hz, 2H), 2.17 – 2.10 (m, 1H), 1.97 (t, *J* = 2.6 Hz, 1H), 1.85 – 1.75 (m, 2H), 1.60 – 1.56 (m, 2H). **^{13}C NMR** (151 MHz, $CDCl_3$) δ 171.1, 169.7, 169.3, 168.3, 167.6, 145.8, 136.4, 132.7, 116.7, 112.7, 111.4, 83.8, 69.1, 65.3, 49.1, 44.6, 31.5, 27.7, 24.9, 22.9, 18.2. **LC-MS (ESI)**, $[M+H]^+$ *m/z*: 412.2.

*Synthesis of hex-5-yn-1-yl 2-(4-(2,6-dioxopiperidin-3-yl)phenoxy)acetate (**15**)*

The *tert*-butyl 2-(4-(2,6-dioxopiperidin-3-yl)phenoxy)acetate (compound **13**, 2.00 g) was synthesized following a previously reported method[26]. To a solution of compound **13** (0.490 g, 1.53 mmol, 1 eq.) in DCM (15 mL) TFA (3 mL) was added, the mixture was stirred at room temperature for 2 h. The complete

removal of *tert*-butyl group was monitored by TLC. Afterwards, the mixture was dried *in vacuo* to provide the crude product for the next step. To a solution of the resulting crude in anhydrous DMF (15 mL) HATU (1.17 g, 3.07 mmol, 2 eq.) and DIPEA (0.595 g, 4.60 mmol, 3 eq.) were added. The mixture was stirred for 30 min at room temperature. Next, hex-5-yn-1-ol (0.301 g, 3.07 mmol, 2 eq.) was added to the reaction mixture and stirred for 15 h. The completion of the reaction was monitored by HPLC. The mixture was poured into water (100 mL) and extracted with ethyl acetate (3 x 30 mL). The combined organic layer was then washed with water (3 x 50 mL) and followed by brine (50 mL), dried over anhydrous Na_2SO_4, filtered, and concentrated *in vacuo* to offer the crude product, which was then purified by silica column (CyH/EtOAc, 1:1, *v/v*) to afford compound **15** (0.364 g, 69%). **^{1}H NMR** (600 MHz, $CDCl_3$) δ 7.99 (s, 1H), 7.17 – 7.10 (m, 2H), 6.95 – 6.87 (m, 2H), 4.62 (s, 2H), 4.24 (t, *J* = 6.5 Hz, 2H), 3.74 (dd, *J* = 9.9, 5.1 Hz, 1H), 2.73 (dt, *J* = 17.7, 5.3 Hz, 1H), 2.64 (ddd, *J* = 17.7, 10.1, 5.2 Hz, 1H), 2.30 – 2.17 (m, 4H), 1.96 (t, *J* = 2.6 Hz, 1H), 1.83 – 1.76 (m, 2H), 1.60 – 1.54 (m, 2H). **^{13}C NMR** (151 MHz, $CDCl_3$) δ 173.3, 172.3, 169.0, 157.5, 130.3, 129.4, 115.3, 83.8, 69.0, 65.5, 65.0, 47.3, 31.1, 27.7, 26.5, 24.9, 18.1. **LC-MS (ESI)**, $[M-H]^-$ *m/z*: 342.1.

*Synthesis of N-(benzyloxy)-4-((2-(6-(2-((2-(2,6-dioxopiperidin-3-yl)-1,3-dioxoisoindolin-4-yl)amino)acetamido)hexyl)-1,2,3,4-tetrahydro-5H-pyrido[4,3-b]indol-5-yl)methyl)benzamide (**16**)*

Prepared by following the **General procedure A**. Starting from de-protected compound **4** (0.197 g, 0.385 mmol, 1 eq.), compound **11** (0.140 g, 0.424 mmol, 1.1 eq.), HATU (0.293 g, 0.770 mmol, 2 eq.) and DIPEA (202 µL, 1.16 mmol, 3 eq.). The crude product was purified by silica column (DCM/MeOH, 20:1, *v/v*, 1% Et_3N) to afford compound **16** (0.279 g, 88%). **^{1}H NMR** (600 MHz, DMSO-d_6) δ 11.66 (s, 1H), 11.08 (s, 1H), 8.06 (t, *J* = 5.7 Hz, 1H), 7.68 – 7.62 (m, 2H), 7.59 (dd, *J* = 8.5, 7.1 Hz, 1H), 7.46 –

7.32 (m, 6H), 7.09 (d, *J* = 8.1 Hz, 2H), 7.06 (d, *J* = 7.1 Hz, 1H), 7.05 – 7.02 (m, 1H), 6.99 (t, *J* = 7.4 Hz, 1H), 6.94 (t, *J* = 5.6 Hz, 1H), 6.86 (d, *J* = 8.5 Hz, 1H), 5.38 (s, 2H), 5.07 (dd, *J* = 12.7, 5.5 Hz, 1H), 4.89 (s, 2H), 3.92 (d, *J* = 5.6 Hz, 2H), 3.65 (s, 2H), 3.10 (q, *J* = 6.6 Hz, 2H), 2.88 (dd, *J* = 5.5, 3.3 Hz, 1H), 2.87 – 2.78 (m, 2H), 2.74 (s, 2H), 2.60 (dd, *J* = 4.6, 2.6 Hz, 1H), 2.59 – 2.55 (m, 2H), 2.53 (dd, *J* = 13.4, 4.5 Hz, 1H), 2.05 – 1.99 (m, 1H), 1.54 (h, *J* = 7.0 Hz, 2H), 1.43 (p, *J* = 7.0 Hz, 2H), 1.35 – 1.21 (m, 4H). **^{13}C NMR** (151 MHz, DMSO-d_6) δ 172.7, 170.0, 168.7, 168.2, 167.3, 163.9, 145.8, 142.1, 136.3, 136.1, 135.9, 133.9, 132.0, 131.2, 128.9, 128.3, 128.2, 127.4, 126.4, 125.3, 120.6, 118.8, 117.4, 110.9, 109.9, 109.5, 76.9, 57.2, 50.2, 49.1, 48.6, 45.4, 45.2, 38.5, 30.9, 29.0, 26.6, 26.3, 22.6, 22.3, 22.1. **LC-MS (ESI)**, $[M+H]^+$ *m/z*: 824.7.

*Synthesis of N-(benzyloxy)-4-((2-(6-(2-(4-(2,6-dioxopiperidin-3-yl)phenoxy)acetamido)hexyl)-1,2,3,4-tetrahydro-5H-pyrido[4,3-b]indol-5-yl)methyl)benzamide (**17**)*

Prepared by following the **General procedure A**. Starting from de-protected compound **4** (0.295 g, 0.578 mmol, 1 eq.), compound **14** (0.152 g, 0.578 mmol, 1 eq.), HATU (0.440 g, 1.16 mmol, 2 eq.) and DIPEA (303 μL, 1.73 mmol, 3 eq.). The crude product was purified by silica column (EtOAc/MeOH, 20:1, *v/v*, 1% Et_3N) to yield compound **17** (0.342 g, 78%). **^{1}H NMR** (600 MHz, $CDCl_3$) δ 8.31 (s, 1H), 7.57 (d, *J* = 8.1 Hz, 2H), 7.46 – 7.37 (m, 3H), 7.36 – 7.32 (m, 2H), 7.17 – 7.07 (m, 4H), 6.97 (d, *J* = 8.1 Hz, 2H), 6.93 – 6.85 (m, 2H), 6.59 (t, *J* = 6.0 Hz, 1H), 5.24 (s, 2H), 4.99 (s, 2H), 4.44 (s, 2H), 3.93 (s, 2H), 3.72 – 3.66 (m, 1H), 3.31 (q, *J* = 6.8 Hz, 2H), 3.10 – 2.97 (m, 2H), 2.80 (s, 2H), 2.73 (d, *J* = 7.8 Hz, 2H), 2.68 (dt, *J* = 17.7, 5.1 Hz, 1H), 2.59 (ddd, *J* = 17.7, 10.2, 5.3 Hz, 1H), 2.25 – 2.19 (m, 1H), 2.19 – 2.13 (m, 1H), 1.70 (d, *J* = 9.5 Hz, 2H), 1.53 (p, *J* = 7.1 Hz, 2H), 1.39 – 1.30 (m, 4H). **^{13}C NMR** (151 MHz, $CDCl_3$) δ 173.4, 172.4, 170.1, 168.2, 156.8, 141.8, 137.0, 135.5, 132.8, 131.3, 130.8, 129.7, 129.4,

128.9, 128.7, 128.6, 127.8, 126.5, 125.7, 121.8, 119.8, 117.9, 115.2, 115.2, 109.4, 78.4, 67.6, 57.0, 50.3, 49.4, 47.2, 46.3, 39.0, 34.6, 31.1, 29.5, 27.0, 26.6, 26.3, 23.5. **LC-MS (ESI)**, $[M+H]^+$ *m/z*: 756.6.

Synthesis of 4-(1-(6-(5-(4-((benzyloxy)carbamoyl)benzyl)-1,3,4,5-tetrahydro-2H-pyrido[4,3-b]indol-2-yl)hexyl)-1H-1,2,3-triazol-4-yl)butyl (2-(2,6-dioxopiperidin-3-yl)-1,3-dioxoisoindolin-4-yl)glycinate ***(18)***

Prepared by following the **General procedure B**. Starting from compound **5** (0.241 g, 0.449 mmol, 1.05 eq.), compound **12** (0.176 g, 0.428 mmol, 1 eq.), ascorbic acid (0.226 g, 1.28 mmol, 3 eq.) and $CuSO_4$ (0.0683 g, 0.428 mmol, 1 eq.). The crude product was purified by flash column chromatography to afford compound **18** (0.239 mg, 59%).

^{1}H NMR (600 MHz, $CDCl_3$) δ 9.68 (s, 1H), 8.73 (s, 1H), 7.62 (d, *J* = 7.8 Hz, 2H), 7.48 (t, *J* = 7.7 Hz, 1H), 7.44 – 7.35 (m, 3H), 7.35 – 7.28 (m, 3H), 7.17 (q, *J* = 8.5 Hz, 2H), 7.11 (dd, *J* = 10.1, 7.1 Hz, 2H), 6.95 (d, *J* = 7.8 Hz, 2H), 6.75 (d, *J* = 8.4 Hz, 1H), 6.67 (t, *J* = 5.8 Hz, 1H), 5.24 (s, 2H), 4.99 (s, 2H), 4.86 (dd, *J* = 12.4, 5.4 Hz, 1H), 4.30 (d, *J* = 7.9 Hz, 2H), 4.18 (s, 2H), 4.02 (d, *J* = 5.7 Hz, 2H), 3.33 (s, 2H), 2.97 (s, 2H), 2.83 – 2.55 (m, 6H), 2.10 – 2.01 (m, 2H), 1.88 (s, 4H), 1.70 (s, 4H), 1.45 – 1.19 (m, 6H). **^{13}C NMR** (151 MHz, $CDCl_3$) δ 171.4, 169.8, 169.3, 168.7, 167.6, 165.6, 145.8, 141.0, 137.2, 136.4, 135.6, 132.6, 131.6, 129.4, 128.8, 128.7, 128.6, 128.1, 126.4, 125.1, 122.7, 120.5, 118.0, 116.9, 112.6, 111.2, 109.8, 78.4, 65.5, 60.6, 55.2, 50.0, 49.7, 49.1, 48.8, 46.5, 44.6, 32.0, 31.5, 29.8, 28.2, 26.2, 25.8, 25.3, 24.5, 22.8. **LC-MS (ESI)**, $[M+H]^+$ *m/z*: 948.7.

Synthesis of 4-(1-(6-(5-(4-((benzyloxy)carbamoyl)benzyl)-1,3,4,5-tetrahydro-2H-pyrido[4,3-b]indol-2-yl)hexyl)-1H-1,2,3-triazol-4-yl)butyl 2-(4-(2,6-dioxopiperidin-3-yl)phenoxy)acetate ***(19)***

Prepared by following the **General procedure B**. Starting from compound **15** (0.163 g, 0.475 mmol, 1 eq.), **5** (0.268 g, 0.498 mmol, 1.05 eq.), ascorbic acid (0.251 g, 1.42 mmol, 3 eq.) and $CuSO_4$ (0.0758 g, 0.475 mmol, 1 eq.). The crude product was purified by flash column chromatography to furnish compound **19** (0.228 g, 54%). **^{1}H NMR** (600 MHz, $CDCl_3$) δ 9.27 (s, 1H), 8.25 (s, 1H), 7.59 (d, *J* = 7.5 Hz, 2H), 7.50 – 7.37 (m, 3H), 7.36 – 7.28 (m, 3H), 7.24 – 7.11 (m, 3H), 7.11 – 7.07 (m, 2H), 6.98 (d, *J* = 7.7 Hz, 2H), 6.87 (d, *J* = 8.2 Hz, 2H), 5.25 (s, 2H), 4.99 (s, 2H), 4.59 (s, 2H), 4.30 (d, *J* = 7.1 Hz, 2H), 4.21 (d, *J* = 5.3 Hz, 2H), 4.00 (s, 2H), 3.68 (dd, *J* = 9.9, 5.0 Hz, 1H), 3.08 (d, *J* = 24.2 Hz, 2H), 2.91 – 2.63 (m, 6H), 2.63 – 2.56 (m, 1H), 2.26 – 2.09 (m, 3H), 1.90 (m, 2H), 1.71 (m, 6H), 1.50 – 1.29 (m, 4H). **^{13}C NMR** (151 MHz, $CDCl_3$) δ 173.4, 172.4, 170.5, 169.1, 157.4, 157.2, 141.6, 137.0, 135.5, 131.4, 130.4, 129.7, 129.4, 129.0, 128.9, 128.7, 128.6, 127.9, 126.5, 125.6, 122.0, 120.9, 120.0, 117.9, 115.2, 109.5, 78.4, 65.6, 65.2, 56.4, 50.2, 49.5, 47.3, 46.5, 46.4, 32.1, 31,6, 31.1, 30.1, 28.2, 26.6, 26.5, 26.2, 25.8, 25.3. **LC-MS (ESI)**, $[M+H]^+$ *m/z*: 880.7.

*Synthesis of N-(benzyloxy)-4-((3-((((6-(2-((2-(2,6-dioxopiperidin-3-yl)-1,3-dioxoisoindolin-4-yl)amino)acetamido)hexyl)(methyl)amino)methyl)-1H-indol-1-yl)methyl)benzamide (**20**)*

Prepared by following the **General procedure A**. Starting from de-protected compound **9** (0.300 g, 0.601 mmol, 1 eq.), compound **11** (0.199 g, 0.601 mmol, 1 eq.), HATU (0.457 g, 1.20 mmol, 2 eq.) and DIPEA (315 μL, 1.80 mmol, 3 eq.). The crude product was purified by silica column (DCM/MeOH, 10:1, *v/v*, 1% Et_3N) to provide compound **20** (0.381 g, 80%). **^{1}H NMR** (600 MHz, DMSO-d_6) δ 11.74 (s, 1H), 11.09 (s, 1H), 9.67 (s, 1H), 8.13 (t, *J* = 5.7 Hz, 1H), 7.82 – 7.74 (m, 2H), 7.68 (d, *J* = 8.0 Hz, 2H), 7.58 (dd, *J* = 8.5, 7.1 Hz, 1H), 7.50 – 7.46 (m, 1H), 7.44 – 7.32 (m, 4H), 7.28 (d, *J* = 8.0 Hz, 2H), 7.20 – 7.11 (m, 2H), 7.06 (d, *J* = 7.1 Hz, 1H), 6.94 (t, *J* = 5.6 Hz, 1H), 6.86 (d, *J* = 8.5 Hz, 1H), 5.53 (s, 2H), 5.06

(dd, *J* = 12.8, 5.5 Hz, 1H), 4.89 (s, 2H), 3.92 (d, *J* = 5.5 Hz, 2H), 3.17 (s, 2H), 3.00 – 2.90 (m, 2H), 2.90 – 2.84 (m, 1H), 2.69 (s, 3H), 2.62 – 2.51 (m, 2H), 2.02 (dtd, *J* = 12.8, 5.2, 2.2 Hz, 1H), 1.68 (s, 2H), 1.41 (t, *J* = 6.8 Hz, 2H), 1.28 – 1.24 (m, 6H). **^{13}C NMR** (151 MHz, DMSO-d_6) δ 172.8, 170.0, 168.7, 168.2, 167.3, 164.0, 145.8, 141.3, 136.2, 135.8, 132.2, 132.0, 131.5, 128.9, 128.3, 128.0, 127.4, 127.0, 122.1, 120.1, 119.0, 118.26, 117.4, 116.3, 114.3, 110.9, 110.7, 109.9, 76.9, 54.1, 49.7, 48.9, 48.6, 45.1, 38.6, 38.3, 31.0, 28.8, 25.8, 25.7, 23.5, 22.1. **LC-MS (ESI)**, $[M+H]^+$ *m/z*: 812.6.

Synthesis of N-(benzyloxy)-4-((3-((((6-(2-(4-(2,6-dioxopiperidin-3-yl)phenoxy)acetamido)hexyl)(methyl)amino)methyl)-1H-indol-1-yl)methyl)benzamide ***(21)***

Prepared by following the **General procedure A**. Starting from de-protected compound **9** (0.722 g, 1.45 mmol, 1 eq.), compound **14** (0.381, 1.45 mmol, 1 eq.), HATU (1.10 g, 2.90 mmol, 2 eq.) and DIPEA (757 μL, 4.34 mmol, 3 eq.). The crude product was purified by silica column (EtOAc/MeOH, 10:1, *v/v*, 1% Et_3N) to provide compound **21** (0.582 g, 54%). **^{1}H NMR** (600 MHz, $CDCl_3$) δ 7.63 (td, *J* = 6.8, 1.7 Hz, 3H), 7.43 – 7.39 (m, 2H), 7.36 – 7.27 (m, 4H), 7.20 – 7.13 (m, 3H), 7.13 – 7.11 (m, 2H), 7.06 (d, *J* = 8.1 Hz, 2H), 6.90 – 6.85 (m, 2H), 6.68 (t, *J* = 6.0 Hz, 1H), 5.27 (s, 2H), 5.00 (s, 2H), 4.34 (s, 2H), 3.94 (s, 2H), 3.71-3.68 (m, 1H), 3.20 (q, *J* = 6.8 Hz, 2H), 2.69 (dt, *J* = 17.7, 5.1 Hz, 1H), 2.64 – 2.60 (m, 1H), 2.57 (q, *J* = 8.0, 6.7 Hz, 2H), 2.42 (s, 3H), 2.22 (ddd, *J* = 14.0, 8.6, 5.1 Hz, 1H), 2.16 (ddd, *J* = 13.8, 10.3, 4.7 Hz, 1H), 1.59 (p, *J* = 7.5 Hz, 2H), 1.43 (p, *J* = 7.2 Hz, 2H), 1.28 (ddd, *J* = 8.5, 5.6, 1.8 Hz, 2H), 1.19 (td, *J* = 8.2, 3.9 Hz, 2H). **^{13}C NMR** (151 MHz, $CDCl_3$) δ 173.4, 172.4, 170.1, 168.4, 156.8, 141.3, 136.4, 135.7, 131.7, 130.8, 129.6, 129.4, 128.8, 128.7, 128.7, 128.6, 127.9, 127.2, 126.9, 122.38, 120.2, 119.1, 115.2, 110.0, 78.3, 67.4, 55.6, 52.0, 49.8, 47.3, 41.3, 38.9, 31.2, 29.3, 26.6, 26.4, 26.2, 26.0. **LC-MS (ESI)**, $[M+H]^+$ *m/z*: 744.5.

*Synthesis of 4-((2-(6-(2-((2-(2,6-dioxopiperidin-3-yl)-1,3-dioxoisoindolin-4-yl)amino)acetamido)hexyl)-1,2,3,4-tetrahydro-5H-pyrido[4,3-b]indol-5-yl)methyl)-N-hydroxybenzamide (**AP1**)*

Prepared by following the **General procedure C**. Starting from compound **16** (0.273 g, 0.332 mmol, 1 eq.), the crude product was purified by reverse phase flash column chromatography to yield compound **AP1** (21.5 mg, 9%). **^{1}H NMR** (600 MHz, DMSO-d_6) δ 11.15 (s, 1H), 11.09 (s, 1H), 9.67 (s, 1H), 9.00 (s, 1H), 8.09 (t, *J* = 5.7 Hz, 1H), 7.72 – 7.64 (m, 2H), 7.60 (dd, *J* = 8.5, 7.1 Hz, 1H), 7.53 (d, *J* = 7.8 Hz, 1H), 7.49 (d, *J* = 8.2 Hz, 1H), 7.19-7.11 (m, 3H), 7.09 (t, *J* = 7.1 Hz, 2H), 6.95 (t, *J* = 5.6 Hz, 1H), 6.87 (d, *J* = 8.5 Hz, 1H), 5.52 (d, *J* = 16.9 Hz, 1H), 5.41 (d, *J* = 16.9 Hz, 1H), 5.07 (dd, *J* = 12.8, 5.5 Hz, 1H), 4.74 – 4.66 (m, 1H), 4.32 (dd, *J* = 14.4, 8.0 Hz, 1H), 3.93 (d, *J* = 5.1 Hz, 2H), 3.83 (dd, *J* = 13.1, 5.5 Hz, 1H), 3.49 (dtd, *J* = 13.2, 9.4, 8.9, 5.9 Hz, 1H), 3.28 – 3.23 (m, 2H), 3.15 – 3.10 (m, 3H), 3.03 (dt, *J* = 17.2, 7.0 Hz, 1H), 2.89 (dddd, *J* = 17.1, 13.8, 5.5, 1.6 Hz, 1H), 2.62 – 2.55 (m, 2H), 2.03 (dtd, *J* = 13.0, 5.4, 2.3 Hz, 1H), 1.76 (dh, *J* = 22.0, 6.6 Hz, 2H), 1.45 (p, *J* = 7.0 Hz, 2H), 1.33 (dq, *J* = 9.5, 5.8 Hz, 4H). **^{13}C NMR** (151 MHz, DMSO-d_6) δ 172.8, 170.0, 168.7, 168.3, 167.3, 163.7, 145.8, 141.0, 136.5, 136.2, 132.1, 131.9, 131.4, 127.2, 126.6, 124.4, 121.9, 119.7, 117.8, 117.4, 111.0, 110.1, 109.9, 102.1, 55.1, 49.3, 48.3, 45.8, 45.6, 45.2, 38.4, 34.4, 31.0, 28.8, 25.8, 25.7, 23.6, 22.1. **HRMS (ESI)**: *m/z* $[M+H]^+$ calcd. for $C_{40}H_{43}N_7O_7$: 734.3297, found: 734.3304.

*Synthesis of 4-(1-(6-(5-(4-(hydroxycarbamoyl)benzyl)-1,3,4,5-tetrahydro-2H-pyrido[4,3-b]indol-2-yl)hexyl)-1H-1,2,3-triazol-4-yl)butyl (2-(2,6-dioxopiperidin-3-yl)-1,3-dioxoisoindolin-4-yl)glycinate (**AP2**)*

Prepared by following the **General procedure C**. Starting from compound **18** (0.146 g, 0.154 mmol, 1 eq.), the crude product was purified by reverse phase flash column chromatography to yield compound **AP2** (16.6 mg, 13%). **^{1}H NMR** (600 MHz, DMSO-d_6) δ 11.09 (s, 1H), 8.98 (s, 1H), 7.82 (d, *J* = 4.5 Hz, 1H), 7.68 – 7.62 (m, 2H), 7.54 (ddd, *J* = 19.6, 8.5, 7.1 Hz, 1H), 7.41 – 7.37 (m, 1H), 7.35 (d, *J* = 8.1 Hz, 1H), 7.16 – 7.05 (m, 3H), 7.05 – 7.01 (m, 1H), 7.01 – 6.92 (m, 2H), 6.92 – 6.85 (m, 1H), 5.37 (s, 2H), 5.07 (dd, *J* = 12.8, 5.5 Hz, 1H), 4.28 (t, *J* = 7.1 Hz, 2H), 4.20 (dd, *J* = 10.0, 6.1 Hz, 2H), 4.12 (h, *J* = 3.2 Hz, 2H), 3.58 (s, 2H), 3.47 (s, 1H), 2.88 (ddd, *J* = 16.9, 13.8, 5.5 Hz, 1H), 2.75 (t, *J* = 5.7 Hz, 2H), 2.71 (d, *J* = 5.5 Hz, 2H), 2.63 – 2.56 (m, 3H), 2.53 (dd, *J* = 14.9, 4.3 Hz, 1H), 2.31 – 2.23 (m, 1H), 2.04 (dtd, *J* = 13.1, 5.4, 2.3 Hz, 1H), 1.80 (p, *J* = 7.2 Hz, 2H), 1.62 (dq, *J* = 6.9, 3.6, 2.8 Hz, 4H), 1.53 (p, *J* = 7.3 Hz, 2H), 1.32 (q, *J* = 7.5 Hz, 2H), 1.26 (ddd, *J* = 14.1, 7.8, 5.2 Hz, 2H). **^{13}C NMR** (151 MHz, DMSO-d_6) δ 172.5, 170.2, 168.7, 167.7, 167.2, 163.9, 146.4, 141.6, 136.2, 136.0, 134.1, 132.0, 131.7, 129.5, 127.2, 126.3, 125.3, 121.6, 120.5, 118.7, 117.7, 117.3, 114.3, 111.2, 109.5, 107.9, 64.4, 57.2, 51.2, 50.3, 49.2, 49.1, 45.3, 43.8, 30.9, 29.7, 27.6, 26.7, 26.3, 25.8, 25.3, 24.5, 22.5, 22.1. **HRMS (ESI)**: *m/z* $[M+H]^+$ calcd. for $C_{46}H_{51}N_9O_8$: 858.3933, found: 858.3920.

*Synthesis of 4-((3-((((6-(2-((2-(2,6-dioxopiperidin-3-yl)-1,3-dioxoisoindolin-4-yl)amino)acetamido)hexyl)(methyl)amino)methyl)-1H-indol-1-yl)methyl)-N-hydroxybenzamide (**AP3**)*

Prepared by following the **General procedure C**. Starting from compound **20** (0.386 g, 0.475 mmol, 1 eq.), the crude product was purified by reverse phase flash column chromatography to yield compound **AP3** (70.0 mg, 20%). **^{1}H NMR** (600 MHz, DMSO-d_6) δ 11.15 (s, 1H), 11.09 (s, 1H), 9.33 (s, 1H), 9.00 (s, 1H), 8.09 (t, *J* = 5.7 Hz, 1H), 7.81 – 7.74 (m, 2H), 7.71 – 7.66 (m, 2H), 7.59 (dd, *J* = 8.5, 7.1 Hz, 1H), 7.50 (d, *J* = 8.1 Hz, 1H), 7.26 (d, *J* = 8.3 Hz, 2H), 7.21 – 7.13 (m, 2H), 7.07 (d, *J* = 7.1 Hz, 1H), 6.94 (t,

J = 5.6 Hz, 1H), 6.86 (d, *J* = 8.6 Hz, 1H), 5.53 (s, 2H), 5.06 (dd, *J* = 12.8, 5.4 Hz, 1H), 4.53 (d, *J* = 13.8 Hz, 1H), 4.41 (d, *J* = 13.1 Hz, 1H), 3.92 (d, *J* = 5.6 Hz, 2H), 3.18 – 3.12 (m, 1H), 3.10 (q, *J* = 6.7 Hz, 2H), 2.96 (s, 1H), 2.89 (ddd, *J* = 17.0, 13.9, 5.5 Hz, 1H), 2.70 (s, 3H), 2.62 – 2.51 (m, 2H), 2.02 (dtd, *J* = 12.8, 5.3, 2.3 Hz, 1H), 1.67 (s, 2H), 1.41 (q, *J* = 6.6 Hz, 2H), 1.31 – 1.22 (m, 4H). **^{13}C NMR** (151 MHz, DMSO-d_6) δ 172.8, 170.0, 168.7, 168.3, 167.3, 163.8, 145.8, 140.8, 136.2, 135.9, 132.2, 132.0, 132.0, 127.9, 127.2, 127.0, 122.1, 120.1, 119.0, 118.4, 117.4, 116.4, 110.9, 110.7, 109.8, 54.2, 49.8, 48.9, 48.6, 45.2, 38.6, 38.3, 31.0, 28.8, 25.8, 25.7, 23.5, 22.1. **HRMS (ESI)**: *m/z* $[M+H]^+$ calcd. for $C_{39}H_{43}N_7O_7$: 722.3297, found: 722.3302.

*Synthesis of 4-((2-(6-(2-(4-(2,6-dioxopiperidin-3-yl)phenoxy)acetamido)hexyl)-1,2,3,4-tetrahydro-5H-pyrido[4,3-b]indol-5-yl)methyl)-N-hydroxybenzamide (**AP4**)*

Prepared by following the **General procedure C**. Starting from compound **17** (0.289 g, 0.382 mmol, 1 eq.), the crude product was purified by reverse phase flash column chromatography to yield compound **AP4** (23.4 mg, 9%). **^{1}H NMR** (600 MHz, DMSO-d_6) δ 11.15 (s, 1H), 10.78 (s, 1H), 9.64 (s, 1H), 9.05 – 8.95 (m, 1H), 8.06 (t, *J* = 5.9 Hz, 1H), 7.72 – 7.65 (m, 2H), 7.51 (dd, *J* = 25.2, 8.0 Hz, 2H), 7.17 – 7.12 (m, 4H), 7.09 (t, *J* = 7.5 Hz, 1H), 6.95 – 6.88 (m, 2H), 5.57 – 5.37 (m, 2H), 4.69 (s, 1H), 4.45 (s, 2H), 4.32 (s, 1H), 3.82 (s, 1H), 3.79 (dd, *J* = 11.5, 4.9 Hz, 1H), 3.52 – 3.41 (m, 1H), 3.25 (s, 2H), 3.15 (q, *J* = 6.7 Hz, 3H), 3.03 (s, 1H), 2.65 (ddd, *J* = 17.2, 11.8, 5.3 Hz, 1H), 2.49 – 2.45 (m, 1H), 2.15 (dtd, *J* = 13.1, 11.7, 4.5 Hz, 1H), 2.00 (dq, *J* = 13.2, 4.8 Hz, 1H), 1.75 (s, 2H), 1.48 (p, *J* = 7.2 Hz, 2H), 1.33 (ddt, *J* = 15.1, 8.8, 5.5 Hz, 4H). **^{13}C NMR** (151 MHz, DMSO-d_6) δ 174.4, 173.4, 167.5, 163.7, 156.6, 141.0, 136.5, 131.9, 131.8, 131.5, 129.5, 127.2, 126.6, 124.4, 121.9, 119.6, 117.8, 114.5, 110.1, 102.2, 67.1, 55.1, 49.4,

48.3, 46.5, 45.6, 38.1, 31.3, 28.8, 26.0, 25.8, 25.7, 23.6, 19.7. **HRMS (ESI)**: *m/z* $[M+H]^+$ calcd. for $C_{38}H_{43}N_5O_6$: 666.3286, found: 666.3292.

*Synthesis of 4-(1-(6-(5-(4-(hydroxycarbamoyl)benzyl)-1,3,4,5-tetrahydro-2H-pyrido[4,3-b]indol-2-yl)hexyl)-1H-1,2,3-triazol-4-yl)butyl 2-(4-(2,6-dioxopiperidin-3-yl)phenoxy)acetate (**AP5**)*

Prepared by following the **General procedure C**. Starting from compound **19** (0.125 g, 0.142 mmol, 1 eq.), the crude product was purified by reverse phase flash column chromatography to yield compound **AP5** (23.9 mg, 21%). **^{1}H NMR** (600 MHz, DMSO-d_6) δ 11.12 (s, 1H), 10.80 (s, 1H), 9.00 (s, 1H), 7.84 (s, 1H), 7.71 – 7.64 (m, 2H), 7.41 (dd, *J* = 7.7, 1.2 Hz, 1H), 7.37 (d, *J* = 8.1 Hz, 1H), 7.16 – 7.11 (m, 2H), 7.09 (d, *J* = 8.3 Hz, 2H), 7.05 (ddd, *J* = 8.2, 7.0, 1.3 Hz, 1H), 7.00 (td, *J* = 7.4, 7.0, 1.0 Hz, 1H), 6.91 – 6.86 (m, 2H), 5.39 (s, 2H), 4.78 (s, 2H), 4.30 (t, *J* = 7.1 Hz, 2H), 4.16 (q, *J* = 4.4, 2.9 Hz, 2H), 3.80 (dd, *J* = 11.6, 4.9 Hz, 1H), 3.60 (s, 2H), 2.77 (t, *J* = 5.7 Hz, 2H), 2.73 (d, *J* = 5.5 Hz, 2H), 2.69 – 2.61 (m, 3H), 2.56 – 2.53 (m, 1H), 2.51 – 2.39 (m, 2H), 2.20 – 2.12 (m, 1H), 2.04 – 1.98 (m, 1H), 1.82 (p, *J* = 7.2 Hz, 2H), 1.64 (p, *J* = 4.0, 3.6 Hz, 4H), 1.55 (p, *J* = 7.3 Hz, 2H), 1.35 (p, *J* = 7.1 Hz, 2H), 1.28 (ddd, *J* = 14.2, 8.1, 5.5 Hz, 2H). **^{13}C NMR** (151 MHz, DMSO-d_6) δ 174.3, 174.3, 173.4, 173.3, 168.8, 156.5, 146.4, 141.6, 136.2, 134.1, 131.8, 131.7, 129.5, 127.2, 126.3, 125.4, 121.6, 120.5, 118.7, 117.4, 114.3, 109.5, 107.9, 64.6, 64.2, 57.2, 50.3, 49.2, 49.1, 46.5, 45.3, 31.3, 29.7, 27.6, 26.7, 26.3, 25.9, 25.8, 25.3, 24.5, 22.5. **HRMS (ESI)**: *m/z* $[M+H]^+$ calcd. for $C_{44}H_{51}N_7O_7$: 790.3923, found: 790.3909.

*Synthesis of 4-((3-((((6-(2-(4-(2,6-dioxopiperidin-3-yl)phenoxy)acetamido)hexyl)(methyl)amino)methyl)-1H-indol-1-yl)methyl)-N-hydroxybenzamide (**AP6**)*

Prepared by following the **General procedure C**. Starting from compound **21** (0.512 g, 0.688 mmol, 1 eq.), the crude was purified by reverse phase flash column chromatography to yield compound **AP6** (0.147 g, 33%). **^{1}H NMR** (600 MHz, DMSO-d_6) δ 11.15 (s, 1H), 10.78 (s, 1H), 9.41 (s, 1H), 9.00 (s, 1H), 8.06 (t, *J* = 5.9 Hz, 1H), 7.82 – 7.73 (m, 2H), 7.72 – 7.65 (m, 2H), 7.50 (d, *J* = 8.3 Hz, 1H), 7.30 – 7.23 (m, 2H), 7.21 – 7.16 (m, 1H), 7.16 – 7.13 (m, 2H), 6.95 – 6.88 (m, 2H), 5.53 (s, 2H), 4.53 (d, *J* = 13.9 Hz, 1H), 4.45 (s, 2H), 4.43 – 4.31 (m, 1H), 3.79 (dd, *J* = 11.5, 4.9 Hz, 1H), 3.20 – 3.08 (m, 3H), 2.97 (s, 1H), 2.70 (s, 3H), 2.65 (ddd, *J* = 17.1, 11.8, 5.3 Hz, 1H), 2.49 – 2.45 (m, 1H), 2.15 (dtd, *J* = 13.1, 11.7, 4.4 Hz, 1H), 2.00 (dq, *J* = 13.2, 4.8 Hz, 1H), 1.68 (q, *J* = 7.9 Hz, 2H), 1.44 (t, *J* = 6.9 Hz, 2H), 1.34 – 1.21 (m, 4H). **^{13}C NMR** (151 MHz, DMSO-d_6) δ 174.4, 173.4, 167.5, 163.8, 156.7, 140.8, 135.9, 132.2, 132.0, 131.8, 129.5, 127.9, 127.2, 127.0, 122.1, 120.1, 119.0, 114.5, 110.7, 102.8, 67.1, 56.0, 54.2, 49.8, 48.9, 46.5, 38.6, 38.0, 31.3, 28.8, 26.0, 25.8, 25.7. **HRMS (ESI)**: *m/z* $[M+H]^+$ calcd. for $C_{37}H_{43}N_5O_6$ 654.3286, found: 654.3290.

Biological and physicochemical evaluation

HDAC inhibition assays

***In vitro* HDAC6 assay.** The *in vitro* inhibitory activity against HDAC6 was measured using our previously published assay protocol[36, 43, 44]. In short, 3-fold serial dilutions of test compounds and controls were prepared in assay buffer (50 mM Tris-HCl (pH 8.0), 137 mM NaCl, 2.7 mM KCl, 1.0 mM $MgCl_2 \cdot 6\ H_2O$, and 0.1 mg/mL BSA). These serial dilutions (5.0 µL) were transferred into 96-well microplates (OptiPlate-96 F, black, PerkinElmer). 35 µL of the fluorogenic substrate ZMAL (Z-Lys(Ac)-AMC; 21.43 µM in assay buffer) and 10 µL of human recombinant HDAC enzyme solution (HDAC6 - BPS Bioscience, Catalog# 50006) in assay buffer were added[45]. The total assay volume of 50 µL (max.

1% DMSO) was incubated at 37 °C for 90 min. Subsequently, 50 µL trypsin solution (0.4 mg/mL trypsin in buffer: 50 mM Tris-HCl (pH 8.0), 100 mM NaCl) was added, followed by 30 min of incubation at 37 °C. Fluorescence (excitation, 355 nm; emission, 460 nm) was measured using a FLUOstar OPTIMA microplate reader (BMG LABTECH). All compounds were tested in duplicate. Reported mean IC_{50}-values, including standard deviation, were calculated from at least two independent experiments.

***In vitro* HDAC10 assay.** HDAC10 inhibition assays were performed by Reaction Biology Corp. (Malvern PA, USA; CAT# HDAC10). In short, either 10 µL of reaction buffer (20 mM Na_2HPO_4 (pH 8.0), 100 mM NaCl, 0.25 mM EDTA, 10 mM Mesna, 0.01% Brij35, 1% DMSO) or 10 µL of human full-length HDAC10 (aa2-669end, Accession #NM_032019.5, N-terminal GST-TEV-tag, expressed in Sf9 insect cells) enzyme solution in reaction buffer was transferred into 384-well microplates (flat bottom, black, Corning® - #3573). Next, 3-fold serial dilutions of test compounds and controls in DMSO were added using acoustic technology (Echo®550 Liquid Handler, BeckmanCoulter; nanoliters) and the mixture was pre-incubated for 20 min. Subsequently, 10 µL of substrate solution (Ac-spermidine-AMC; final assay concentration: 12.5 µM) in reaction buffer was added and the final assay volume of 20 µL was incubated at 30 °C. After 1 h of incubation time, "stop"-solution (borate buffer (pH 9.5), NDA; final assay concentration: 167 µM) was added. Fluorescence (excitation, 355 nm; emission, 460 nm) was measured using an EnVision microplate reader (PerkinElmer). All compounds were tested in duplicate. Reported mean IC_{50}-values, including standard deviation, were calculated from at least two independent experiments.

CRBN target engagement assay

The assay was performed as previously described by Zerfas et al.[31] HEK293T cells stably expressing NanoLuc-CRBN were cultured in DMEM (Gibco, Life Technologies) supplemented with 10% FBS. Cells were resuspended at 2 x 10^5 cells/mL in 21 mL Opti-MEM I (Gibco, Life Technologies) and mixed with 600 µL BODIPY™-lenalidomide fluorescent tracer (stock at 10 µM diluted in tracer dilution buffer 31.25% PEG-400, 12.5 mM HEPES, pH 7.5, filtered using a 0.22 µm nitrocellulose membrane) to reach final concentration of the tracer at 278 nM. The cell-tracer mixture was then plated in a white polystyrene 384-well plate (Corning, 3570) at 50 µL/well. After plating, the assay plate was centrifuged (400 x g, 5 min) and protected from light. Compounds for testing were added to the plate using a D300e Digital Dispenser (Tecan) in duplicate 12-pt titrations from a 10 mM stock in DMSO, with DMSO normalized to 1% total volume. The plate was then placed in an incubator at 37 °C, 5% CO_2 for two hours. After incubation, the plate was removed and set on the bench to cool to room temperature (~10 min). The NanoLuc substrate (500X solution, Promega Catalog number N2160 for 1,000 assay kit) and extracellular inhibitor (1500X solution, Promega Catalog number N2160 for 1,000 assay kit) were diluted in Opti-MEM I (Gibco, Life Technologies) to prepare a 3X solution, which was added to each well (25 µL/well). The plate was read on a Pherastar FSX (BMG Labtech) microplate reader with simultaneous dual emission capabilities at 450 and 520 nm for 10 cycles. The NanoBRET ratio was calculated by dividing the signal at 520 nm by the signal at 450 nm and multiplying by 1000 for each sample and averaged across 10 read cycles to create each data point. The data was plotted in GraphPad Prism 10 and the curves were fitted using Variable Slope equation to obtain the EC_{50} values.

Determination of Physicochemical Properties

LogD$_{7.4}$ Measurements. The determination of the log$D_{7.4}$ values was performed by a chromatographic method as described previously[46]. Briefly, the system was calibrated by plotting the retention times of six different drugs (atenolol, metoprolol, labetalol, diltiazem, triphenylene, permethrin) versus their literature known log$D_{7.4}$ values to obtain a calibration line ($R^2 \geq 0.95$). Subsequently, the mean retention times of the analytes were taken to calculate their log$D_{7.4}$ values with aid of the calibration line.

Plasma Protein Binding Studies. PPB was estimated by correlating the logarithmic retention times of the analytes on a CHIRALPAK HSA 50 × 3 mm, 5 µm column with the literature known %PPB values (converted into log$K$ values) of the following drugs: warfarin, ketoprofen, budesonide, nizatidine, indomethacin, acetylsalicylic acid, carbamazepine, piroxicam, nicardipine, and cimetidine. Samples were dissolved in MeCN/DMSO 9:1 to achieve a final concentration of 0.5 mg/mL. The mobile phase A was 50 mM NH_4Ac adjusted to *p*H 7.4 with ammonia, while mobile phase B was *i*PrOH. The flow rate was set to 1.0 mL/min, the UV detector was set to 254 nm, and the column temperature was kept at 30 °C. After injecting 3 µL of the sample, a linear gradient from 100% A to 30% *i*PrOH in 5.4 min was applied. From 5.4 to 18 min, 30% *i*PrOH was kept, followed by switching back to 100% A in 1.0 min and a re-equilibration time of 6 min. With the aid of the calibration line ($R^2 \geq 0.92$), the log$K$ values of new substances were calculated and converted to their %PPB values.

Molecular Descriptor Calculations. Calculated values for the topological polar surface area (TPSA) and number of rotatable bonds (NRotB) were determined using the free web tool SwissADME[47].

Western blotting

Western blots on HDAC1, 4, 6, 8, 10, acetylated histone H3, acetylated α-tubulin and GAPDH in MM.1S cells, as well as the HDAC6, 10 and GAPDH in MCF-7 cells were performed according to a previously

published protocol[48-50]. In brief, MM.1S or MCF-7 were collected and lysed with cell extraction buffer (ThermoFisher Scientific Inc.; Waltham, MA, USA), supplemented with 0.1 mM PMSF, Halt™ Protease Inhibitor (Thermo Fisher), and sodium orthovanadate (ThermoFisher Scientific Inc.; Waltham, MA, USA). Protein concentration was determined using a BCA kit (ThermoFisher Scientific Inc.; Waltham, MA, USA). Equal amounts of protein (25 µg) from the lysates was denatured by Laemmli 2× Concentrate (Catalog# S3401-10VL, Sigma-Aldrich, St. Louis, MO, USA), and Precision Plus Protein Unstained Standard was used as molecular weight marker (Catalog# 1610363, Bio-Rad, Hercules, CA, USA). SDS-PAGE was performed with precast gels with a polymerization degree of 4-15% (for ac-histone H3) and 10% or 12% for other proteins (Mini-PROTEAN® TGX™ Stain-Free™; Bio-Rad Laboratories GmbH, Germany). Afterward, proteins were transferred to Trans-Blot Turbo®-PVDF membranes (Bio-Rad). The membrane was blocked with skimmed milk powder in Tris-buffered saline-Tween 20 (with 0.2% Tween 20) for 60 min, followed by three washing cycles of 10 min using Tris-buffered saline-Tween 20. Next, membranes were incubated with primary antibodies for a total of 60 min at room temperature under slight agitation and then incubated at 4 °C overnight. Membranes were rinsed again three times before applying the secondary anti-rabbit IgG HRP-conjugated mAbs (R&D Systems, Inc., Minneapolis, USA) or anti-mouse IgG HRP-conjugated mAbs (Santa Cruz Biotechnology, Texas, USA) for 90 min. After rinsing of the secondary antibody, membranes were detected using the ClarityECL Western Blotting Substrate (Bio-Rad). For quantitative determination, the StainFree technique was employed (Bio-Rad), as well as normalization, against the housekeeping protein GAPDH, which allows the imaging of whole lysates in SDS-PAGE before blotting and normalization against the total protein. Pixel density analysis was performed with the IMAGE LAB software (Bio-Rad). Primary antibodies were used as antibody solutions in 1:1000–1:20000 dilutions. Anti-HDAC1 (Catalog#

5356S, Cell Signaling Technology, Denver, MA, USA), anti-HDAC4 (Catalog#7628S, Cell Signaling Technology, Denver, MA, USA), anti-HDAC6 (Catalog#7558S, Cell Signaling Technology, Denver, MA, USA), anti-acetyl-histone H3 (Catalog#9677S, Cell Signaling Technology, Denver, MA, USA), anti-acetyl-α-tubulin (Catalog#5335, Cell Signaling Technology, Denver, MA, USA), anti-HDAC8 (Catalog#66042S, Cell Signaling Technology, Denver, MA, USA), anti-HDAC10 (Catalog#H3413, Sigma-Aldrich, St. Louis, MO, USA), anti-GAPDH (Catalog# T0004, Affinity Biosciences, Cincinnati, OH, USA).

Cell viability assays

Cell culture. MM.1S cells were obtained by the American Type Culture Collection (ATCC, Manassas, VA, USA). Cells were cultured in RPMI 1640 (Life Technologies, Darmstadt, Germany) supplemented with 10 % fetal bovine serum (PAN Biotech GmbH, Aidenbach, Germany), 100 IU/mL penicillin and 0.1 mg/mL streptomycin (PAN Biotech GmbH, Aidenbach, Germany) and 1 mM sodium pyruvate (ThermoFisher Scientific Inc.; Waltham, MA, USA) and were incubated at 37 °C under humidified air with 5% CO_2. MCF-7 cells were obtained by the American Type Culture Collection (ATCC, Manassas, VA, USA). Cells were cultured in Dulbecco's Modified Eagle's Medium (DMEM, Gibco) already containing L-glutamine and pyruvate, and supplemented with 10 % fetal bovine serum (PAN Biotech GmbH, Aidenbach, Germany), 100 IU/mL penicillin and 0.1 mg/mL streptomycin (PAN Biotech GmbH, Aidenbach, Germany), and were incubated at 37 °C under humidified air with 5% CO_2.

CellTiterGlo® 2.0 assay in MM.1S cells. 2,500 MM.1S cells/well were seeded in white 384-well plates (Greiner Bio-One, Kremsmuenster, Austria). The final assay volume was 25 µL. A 200-fold dilution series was prepared in DMSO and further diluted to 10-fold in medium and added to the cells. The final

DMSO concentration was 0.5%. The toxicity of compounds was determined after 72 h using the CellTiter-Glo® 2.0 Cell Viability Assay (Promega, Madison, WI, USA, #G9242) according to the manufacturer's protocol. Subsequently, the luminescence was measured using a Tecan Spark (Tecan Group AG, Maennedorf, Swiss). Data was analyzed with the four-parameter logistic equation (GraphPad Prism 9.0, San Diego, CA, USA).

MTT assay in MCF-7 cells. Assays were conducted following previously reported methods. [43] MTT (3-(4,5-dimethylthiazol-2-yl)-2,5-diphenyltetrazolium bromide; Catalog# A2231; BioChemica, Applichem GmbH, Darmstadt, Germany) was used to measure cell viability. A total of 2,500 MCF-7 cells were seeded in triplicates in 96-well plates (Starlab GmbH, Hamburg, Germany) with each well containing 200 µL of volume. These cells were subsequently treated with dilution series of different compounds. Following an incubation period of 72 hours, 20 µL of freshly prepared MTT solution (5 mg/mL) was added and the mixture was incubated for 1 hour at 37 °C and 5% CO_2. After removing the supernatant, the formazan dye was solubilized in 200 µL DMSO (Sigma-Aldrich, Steinheim, Germany). The absorbance was determined at 570 nm with background subtraction at 690 nm by a microplate photometer (Thermo Scientific Multiskan EX, Thermo Fisher Sceintific). The acquired data was normalized to DPBS, considering 100% viability, and the half-maximal inhibitory concentration (IC50) was determined by plotting dose response curves and nonlinear regression with GraphPad Prism (GraphPad Software, San Diego, CA, USA).

Quantitative proteomics (MM.1S cells)

Sample preparation for whole-proteome analysis. 2 million MM.1S cells were seeded in a T25 flask in 7 mL media the day before giving the treatments. After incubating for 24 h, 7 µL of DMSO or

compounds in 10 mM stock solutions were given to the cells and the incubated for 6 h. The cells were collected and washed with DPBS twice, aspirate off DPBS and the cell pellets were frozen with liquid nitrogen and stored in -80 °C.

Frozen MM1.S cell pellets were lysed in 200 uL of urea lysis buffer (6 M urea, 2 M thiourea in 50 mM TRIS-HCl pH=8.5). To degrade chromatin 7.5 U/mL of Benzonase (ThermoFisher Scientific Inc.; Waltham, MA, USA) was added to the samples before incubation for 10 min on ice. Samples were centrifuged for 10 min at 15000xg. Supernatants were transferred to new tubes and the concentration was determined using Pierce™ 660 nm Protein Assay Reagent (ThermoFisher Scientific Inc.; Waltham, MA, USA). Subsequently, urea concentration was reduced to 2 M and 100 ug of protein per sample was used for further processing. To reduce and alkylate cysteine bonds, 10 mM TCEP bond-breaker™ solution (ThermoFisher Scientific Inc.; Waltham, MA, USA) and 40 mM chloroacetamide were added simultaneously and incubated for 30 min at room temperature in the dark. Overnight digestion was carried out at room temperature by adding of 1 µg Trypsin/LysC per 100 ug of protein. Digestion was stopped by adding stop buffer (20% acetonitrile in ddH_2O and 6% TFA), followed by desalting of 40 ug of peptides on poly(styrene-divinylbenzene) reverse-phase sulfonated (SDB-RPS) plugs stacked in 200 µL pipet tips. Peptides were eluted with 50 uL of elution buffer (80% acetonitrile, 15% ddH_2O, 5% ammonia) per sample. Eluents were evaporated at 30 °C for 2 h. Dried peptides were resuspended in 12 µL of loading buffer (2% acetonitrile in 0.1% FA ddH_2O). Before application to the mass spectrometer, the concentration of each sample was adjusted to 300 ng/µL.

LC-MS/MS. Peptides in buffer A (0.1% FA in ddH_2O) were separated using a NeoVanquish HPLC system (ThermoFisher Scientific Inc.; Waltham, MA, USA) with a 25 cm Aurora Ultimate column (C18, 75 µm inner diameter) coupled to an Exploris 480 mass spectrometer (ThermoFisher Scientific Inc.;

Waltham, MA, USA) via a nanoelectrospray source. Peptides were separated with a 90 min gradient, starting with 6% buffer B (80% acetonitrile, 0.1% FA in ddH_2O) increasing linearly to 25% after 70 min, followed by stepwise increase to 55% buffer B (78 min) and 95% buffer B (90 min) at a flowrate of 300 nL/min and a column temperature of 55 °C. A staggered, data-independent mass spectrometry method was used with a full MS scan ranging from 380 – 1020 m/z (resolution = 60000, injection time = 55 ms, AGC target = 100). Each full MS scan was followed by 50 DIA scans spanning 400 – 1000 m/z (window size 12 m/z, resolution = 30000, ion fill time =55 ms, AGC target = 1000).

Gas-phase fractionation library. To create a sample-specific gas-phase-fractionation library 1 µL of each sample was pooled and six MS measurements form this pool were recorded. Each individual measurement covered a different m/z-window of 100, spanning in total a range between 400 and 1000 m/z. The library was created with DIA-NN software (version 1.8.1) using a *homo sapiens* FASTA file (UniProt file form the 18.11.2021).

Identification, quantification and statistical analysis. The raw files obtained from the mass spectrometer were de-staggered using MSconvert (64-bit). Prior to processing of raw files, the run-specific mass accuracies for MS1 and MS2 and the scan windows were determined using DIAN-NN (version 1.8.1) with precursor FDR set to 1% and log-level set to 1. The MS raw files were processed by DIA-NN software (version 1.8.1) using the generated gas-phase fractionation library as reference (FDR = 1%, Scan window radius = 12, MS1 accuracy = 4.0×10^{-6}, MS2 accuracy 1.7×10^{-5}) and processed files were MaxLFQ normalized. Data was log-transformed and contaminants were removed. Protein groups were filtered based on 100% data completeness in at least one group. Missing values were replaced samples wise based on a random selection of values from a normal distribution (mean = downshifted 1.8 standard deviations, SD = 0.3). Determination of significant up- or downregulations was

carried out by using a two-sample Welch's T-test (FDR =0.05). Fold changes (x-axis) and p-values (y-axis) were plotted against each other for each condition vs. DMSO and depicted as volcano plots.

Quantitative proteomics (MOLT4 cells)

Sample preparation LFQ quantitative mass spectrometry. Cells were lysed by addition of lysis buffer (8 M Urea, 50 mM NaCl, 50 mM 4-(2-hydroxyethyl)-1-piperazineethanesulfonic acid (EPPS) pH 8.5, Protease and Phosphatase inhibitors) and homogenization by bead beating (BioSpec) for three repeats of 30 seconds at 2400 strokes/min. Bradford assay was used to determine the final protein concentration in the clarified cell lysate. Fifty micrograms of protein for each sample was reduced, alkylated and precipitated using methanol/chloroform as previously described [51] and the resulting washed precipitated protein was allowed to air dry. Precipitated protein was resuspended in 4 M urea, 50 mM HEPES pH 7.4, followed by dilution to 1 M urea with the addition of 200 mM EPPS, pH 8. Proteins were digested with the addition of LysC (1:50; enzyme:protein) and trypsin (1:50; enzyme:protein) for 12 h at 37 °C. Sample digests were acidified with formic acid to a pH of 2-3 before desalting using C18 solid phase extraction plates (SOLA, Thermo Fisher Scientific). Desalted peptides were dried in a vacuum-centrifuged and reconstituted in 0.1% formic acid for liquid chromatography-mass spectrometry analysis. Data were collected using a TimsTOF HT (Bruker Daltonics, Bremen, Germany) coupled to a nanoElute LC pump (Bruker Daltonics, Bremen, Germany) via a CaptiveSpray nano-electrospray source. Peptides were separated on a reversed-phase C18 column (25 cm x 75 µm ID, 1.6 µM, IonOpticks, Australia) containing an integrated captive spray emitter. Peptides were separated using a 50 min gradient of 2 - 30% buffer B (acetonitrile in 0.1% formic acid) with a flow rate of 250 nL/min and column temperature maintained at 50 ºC. The TIMS elution voltages were calibrated linearly with three points (Agilent ESI-L Tuning Mix

Ions; 622, 922, 1,222 *m/z*) to determine the reduced ion mobility coefficients ($1/K_0$). To perform diaPASEF, we used py_diAID[52], a python package, to assess the precursor distribution in the *m/z*-ion mobility plane to generate a diaPASEF acquisition scheme with variable window isolation widths that are aligned to the precursor density in *m/z*. Data was acquired using twenty cycles with three mobility window scans each (creating 60 windows) covering the diagonal scan line for doubly and triply charged precursors, with singly charged precursors able to be excluded by their position in the m/z-ion mobility plane. These precursor isolation windows were defined between 350 - 1250 *m/z* and $1/k_0$ of 0.6 - 1.45 $V.s/cm^2$.

LC-MS data analysis. The diaPASEF raw file processing and controlling peptide and protein level false discovery rates, assembling proteins from peptides, and protein quantification from peptides were performed using library free analysis in DIA-NN 1.8 [53]. Library free mode performs an *in silico* digestion of a given protein sequence database alongside deep learning-based predictions to extract the DIA precursor data into a collection of MS2 spectra. The search results are then used to generate a spectral library which is then employed for the targeted analysis of the DIA data searched against a Swissprot human database (January 2021). Database search criteria largely followed the default settings for directDIA including: tryptic with two missed cleavages, carbamidomethylation of cysteine, and oxidation of methionine and precursor Q-value (FDR) cut-off of 0.01. Precursor quantification strategy was set to Robust LC (high accuracy) with RT-dependent cross run normalization. Proteins with low sum of abundance (<2,000 x no. of treatments) were excluded from further analysis and resulting data was filtered to only include proteins that had a minimum of 3 counts in at least 4 replicates of each independent comparison of treatment sample to the DMSO control. Protein abundances were scaled using in-house scripts in the R framework (R Development Core Team, 2014) and proteins with missing

values were imputed by random selection from a Gaussian distribution either with a mean of the non-missing values for that treatment group or with a mean equal to the median of the background (in cases when all values for a treatment group are missing). Significant changes comparing the relative protein abundance of these treatment to DMSO control comparisons were assessed by moderated t test as implemented in the limma package within the R framework[54].

Molecular docking and ternary complex modeling

Molecular docking was performed in MOE software (version 2022). The crystal structures of HDAC6 (PDB ID: 6THV), HDAC10 (PDB ID: 6WBQ), as well as the cereblon (PDB ID: 8OIZ) were obtained from the Protein Data Bank. Briefly, the chemical structures of docked and modeled molecules were prepared and optimized based on the MMFF94X force field. The receptors (HDAC6, HDAC10 and cereblon crystal complexes) were processed as follows: removal of water molecules, addition of hydrogen atoms and partial charges, protonation based on the Amber10:EHT force field. For docking analysis, the binding site of the native ligand in each receptor was used to define the docking sites. Other MOE-docking parameters were set to default values and 30 predicted poses were retained during the docking process. The best poses of Tubastatin A and its hexyl chain attached-derivative were kept based upon the docking score and the results from ligand interactions, followed by visually inspection. For ternary complex modeling, the method 4B was conducted in the software by submitting the prepared POI, celeblon, as well as the degrader. The best pose was kept in based on the modeling score and the result from ligand interactions, followed by visually inspection. The Figures were generated using the PyMOL software (https://pymol.org/2/).

PAINS Analysis

We filtered all compounds for pan-assay interference compounds (PAINS) using the online filter http://zinc15.docking.org/patterns/home/. No compound was flagged as PAINS.

ASSOCIATED CONTENT

Supporting information

Electronic Supplementary Information (ESI) available: Figures for viability assay on MM.1S and MCF-7 cells; degradation of HDAC6 and HDAC10 by **AP1-AP6** in MCF-7 cells; quantitative proteomics of MM.1S cell lysates after treatment with 1 μM of **AP1** or tubastatin A for 6 hours; synthesis of non-degrading control AP1-N; ^{1}H and ^{13}C NMR spectra of **AP1-AP6**, **AP1-N**; HPLC chromatograms of **AP1-AP6**, **AP1-N** (PDF).

Molecular strings formula (CSV).

AUTHOR INFORMATION

Corresponding Author

Finn K. Hansen Department of Pharmaceutical and Cell Biological Chemistry, Pharmaceutical Institute, University of Bonn, Bonn 53121, Germany. Email: finn.hansen@uni-bonn.de

Authors

Shiyang Zhai Department of Pharmaceutical and Cell Biological Chemistry, Pharmaceutical Institute, University of Bonn, Bonn 53121, Germany.

Linda Schäker-Hübner Department of Pharmaceutical and Cell Biological Chemistry, Pharmaceutical Institute, University of Bonn, Bonn 53121, Germany.

Maria Hanl Department of Pharmaceutical and Cell Biological Chemistry, Pharmaceutical Institute, University of Bonn, Bonn 53121, Germany.

Lukas Jacobi Institute of Innate Immunity, Department of Systems Immunology and Proteomics, Medical Faculty, University of Bonn, Bonn 53127, Germany.

Dominika E. Pieńkowska Institute of Structural Biology, Medical Faculty, University of Bonn, Bonn 53127, Germany.

Jan Gerhartz Institute of Structural Biology, Medical Faculty, University of Bonn, Bonn 53127, Germany.

Rabea Voget Department of Pharmaceutical and Medicinal Chemistry, Pharmaceutical Institute, University of Bonn, Bonn 53121, Germany.

Michael Gütschow Department of Pharmaceutical and Medicinal Chemistry, Pharmaceutical Institute, University of Bonn, Bonn 53121, Germany.

Felix Meissner Institute of Innate Immunity, Department of Systems Immunology and Proteomics, Medical Faculty, University of Bonn, Bonn 53127, Germany.

Radosław P. Nowak Institute of Structural Biology, Medical Faculty, University of Bonn, Bonn 53127, Germany.

Christian Steinebach Department of Pharmaceutical and Medicinal Chemistry, Pharmaceutical Institute, University of Bonn, Bonn 53121, Germany.

ORCID

Shiyang Zhai: 0009-0005-6840-3177

Linda Schäker-Hübner: 0000-0001-7734-124X

Jan Gerhartz: 0009-0002-9457-4656

Rabea Voget: 0009-0003-9249-8773

Michael Gütschow: 0000-0002-9376-7897

Felix Meissner: 0000-0003-1000-7989

Radosław P. Nowak: 0000-0002-0605-0071

Christian Steinebach: 0000-0001-5638-1955

Finn K. Hansen: 0000-0001-9765-5975

Author Contributions

The manuscript was written through contributions of all authors. All authors have given approval to the final version of the manuscript.

Notes

The authors declare no competing financial interest.

Data Deposition

Global proteomics data will be publicly available at the Fischer Lab's Proteomics database: https://proteomics.fischerlab.org.

ACKNOWLEDGEMENTS

S. Z. is funded by China Scholarship Council (grant no. 202106150022). The work of R.V., M.G., C.S., and F.K.H. was funded by the Deutsche Forschungsgemeinschaft (DFG, German Research Foundation)–GRK2873 (494832089). We thank Katherine A. Donovan, Eric S. Fischer and the Fischer Lab Degradation Proteomics Initiative for collection of the global proteomics data supported by NIH

CA214608 and CA218278 (quantitative proteomics in MOLT4 cells). The new NMR console for the 500 MHz NMR spectrometer used in this research was funded by the Deutsche Forschungsgemeinschaft (DFG, German Research Foundation) under project number 507275896.

ABBREVIATIONS

NAD^+, nicotinamide adenine dinucleotide; PDB, protein data bank; HATU, 1-[Bis(dimethylamino)methylene]-1H-1,2,3-triazolo[4,5-b]pyridinium 3-oxide hexafluorophosphate; DCM, dichlorometane; DIPEA, N,N-diisopropylethylamine; DMF, N,N-dimethylformamide; EtOAc, ethyl acetate; LiOH, lithium hydroxide; THF, tetrahydrofuran; HCl, hydrogen chloride; NanoBRET, nano bioluminescence resonance energy transfer; NanoLuc-CRBN, Nano-luciferase cereblon; BODIPY, 5,5-Difluoro-5*H*-4λ^5-dipyrrolo[1,2-*c*:2′,1′-*f*][1,3,2]diazaborinin-4-ylium-5-uide.

References

(1) Kaur, S.; Rajoria, P.; Chopra, M. HDAC6: A unique HDAC family member as a cancer target. *Cell Oncol (Dordr)* **2022**, *45* (5), 779-829.

(2) Arrar, M.; Turnham, R.; Pierce, L.; de Oliveira, C. A.; McCammon, J. A. Structural insight into the separate roles of inositol tetraphosphate and deacetylase-activating domain in activation of histone deacetylase 3. *Protein Sci* **2013**, *22* (1), 83-92.

(3) Ho, T. C. S.; Chan, A. H. Y.; Ganesan, A. Thirty Years of HDAC Inhibitors: 2020 Insight and Hindsight. *J Med Chem* **2020**, *63* (21), 12460-12484.

(4) Chen, X.; He, Y.; Fu, W.; Sahebkar, A.; Tan, Y.; Xu, S.; Li, H. Histone Deacetylases (HDACs) and Atherosclerosis: A Mechanistic and Pharmacological Review. *Front Cell Dev Biol* **2020**, *8*, 581015.

(5) Yang, F.; Zhao, N.; Ge, D.; Chen, Y. Next-generation of selective histone deacetylase inhibitors. *RSC Adv* **2019**, *9* (34), 19571-19583.

(6) Wang, X. X.; Wan, R. Z.; Liu, Z. P. Recent advances in the discovery of potent and selective HDAC6 inhibitors. *Eur J Med Chem* **2018**, *143*, 1406-1418.

(7) Li, Y.; Sang, S.; Ren, W.; Pei, Y.; Bian, Y.; Chen, Y.; Sun, H. Inhibition of Histone Deacetylase 6 (HDAC6) as a therapeutic strategy for Alzheimer's disease: A review (2010-2020). *Eur J Med Chem* **2021**, *226*, 113874.

(8) Yang, K.; Song, Y.; Xie, H.; Wu, H.; Wu, Y. T.; Leisten, E. D.; Tang, W. Development of the first small molecule histone deacetylase 6 (HDAC6) degraders. *Bioorg Med Chem Lett* **2018**, *28* (14), 2493-2497.

(9) An, Z.; Lv, W.; Su, S.; Wu, W.; Rao, Y. Developing potent PROTACs tools for selective degradation of HDAC6 protein. *Protein Cell* **2019**, *10* (8), 606-609.

(10) Wu, H.; Yang, K.; Zhang, Z.; Leisten, E. D.; Li, Z.; Xie, H.; Liu, J.; Smith, K. A.; Novakova, Z.; Barinka, C.; Tang, W. Development of Multifunctional Histone Deacetylase 6 Degraders with Potent Antimyeloma Activity. *J Med Chem* **2019**, *62* (15), 7042-7057.

(11) Yang, H.; Lv, W.; He, M.; Deng, H.; Li, H.; Wu, W.; Rao, Y. Plasticity in designing PROTACs for selective and potent degradation of HDAC6. *Chem Commun (Camb)* **2019**, *55* (98), 14848-14851.

(12) Yang, K.; Wu, H.; Zhang, Z.; Leisten, E. D.; Nie, X.; Liu, B.; Wen, Z.; Zhang, J.; Cunningham, M. D.; Tang, W. Development of Selective Histone Deacetylase 6 (HDAC6) Degraders Recruiting Von Hippel-Lindau (VHL) E3 Ubiquitin Ligase. *ACS Med Chem Lett* **2020**, *11* (4), 575-581.

(13) Yang, K.; Zhao, Y.; Nie, X.; Wu, H.; Wang, B.; Almodovar-Rivera, C. M.; Xie, H.; Tang, W. A Cell-Based Target Engagement Assay for the Identification of Cereblon E3 Ubiquitin Ligase Ligands and

Their Application in HDAC6 Degraders. *Cell Chem Biol* **2020**, *27* (7), 866-876 e868.

(14) Cao, Z.; Gu, Z.; Lin, S.; Chen, D.; Wang, J.; Zhao, Y.; Li, Y.; Liu, T.; Li, Y.; Wang, Y.; Lin, H.; He, B. Attenuation of NLRP3 Inflammasome Activation by Indirubin-Derived PROTAC Targeting HDAC6. *ACS Chem Biol* **2021**, *16* (12), 2746-2751.

(15) Sinatra, L.; Yang, J.; Schliehe-Diecks, J.; Dienstbier, N.; Vogt, M.; Gebing, P.; Bachmann, L. M.; Sö nnichsen, M.; Lenz, T.; Stühler, K.; Schöler A.; Borkhardt A.; Bhatia, S.; Hansen, F. K. Solid-Phase Synthesis of Cereblon-Recruiting Selective Histone Deacetylase 6 Degraders (HDAC6 PROTACs) with Antileukemic Activity. *J Med Chem* **2022**, *65* (24), 16860-16878.

(16) Keuler, T.; König, B.; Bückreiss, N.; Kraft, F. B.; König, P.; Schäker-Hübner, L.; Steinebach, C.; Bendas, G.; Gütschow, M.; Hansen, F. K. Development of the first non-hydroxamate selective HDAC6 degraders. *Chem Commun (Camb)* **2022**, *58* (79), 11087-11090.

(17) Hai, Y.; Shinsky, S. A.; Porter, N. J.; Christianson, D. W. Histone deacetylase 10 structure and molecular function as a polyamine deacetylase. *Nat Commun* **2017**, *8*, 15368.

(18) Shinsky, S. A.; Christianson, D. W. Polyamine Deacetylase Structure and Catalysis: Prokaryotic Acetylpolyamine Amidohydrolase and Eukaryotic HDAC10. *Biochemistry* **2018**, *57* (22), 3105-3114.

(19) Herbst-Gervasoni, C. J.; Christianson, D. W. Binding of N(8)-Acetylspermidine Analogues to Histone Deacetylase 10 Reveals Molecular Strategies for Blocking Polyamine Deacetylation. *Biochemistry* **2019**, *58* (49), 4957-4969.

(20) Lambona, C.; Zwergel, C.; Fioravanti, R.; Valente, S.; Mai, A. Histone deacetylase 10: A polyamine deacetylase from the crystal structure to the first inhibitors. *Curr Opin Struct Biol* **2023**, *82*, 102668.

(21) Cheng, F.; Zheng, B.; Wang, J.; Zhao, G.; Yao, Z.; Niu, Z.; He, W. Histone deacetylase 10, a potential epigenetic target for therapy. *Biosci Rep* **2021**, *41* (6).

(22) Pettersson, M.; Crews, C. M. PROteolysis TArgeting Chimeras (PROTACs) - Past, present and future. *Drug Discov Today Technol* **2019**, *31*, 15-27.

(23) Shen, S.; Svoboda, M.; Zhang, G.; Cavasin, M. A.; Motlova, L.; McKinsey, T. A.; Eubanks, J. H.; Barinka, C.; Kozikowski, A. P. Structural and in Vivo Characterization of Tubastatin A, a Widely Used Histone Deacetylase 6 Inhibitor. *ACS Med Chem Lett* **2020**, *11* (5), 706-712.

(24) Herbst-Gervasoni, C. J.; Steimbach, R. R.; Morgen, M.; Miller, A. K.; Christianson, D. W. Structural Basis for the Selective Inhibition of HDAC10, the Cytosolic Polyamine Deacetylase. *ACS Chem Biol* **2020**, *15* (8), 2154-2163.

(25) Géraldy, M.; Morgen, M.; Sehr, P.; Steimbach, R. R.; Moi, D.; Ridinger, J.; Oehme, I.; Witt, O.; Malz, M.; Nogueira, M. S.; Koch, O.; Gunkel, N.; Miller, A.K. Selective Inhibition of Histone Deacetylase 10: Hydrogen Bonding to the Gatekeeper Residue is Implicated. *J Med Chem* **2019**, *62* (9), 4426-4443.

(26) Min, J.; Mayasundari, A.; Keramatnia, F.; Jonchere, B.; Yang, S. W.; Jarusiewicz, J.; Actis, M.; Das, S.; Young, B.; Slavish, J.; Yang, L.; Li, Y.; Fu, X.; Garrett, S.H.; Yun, M.K.; Li, Z.; Nithianantham, S.; Chai, S.; Chen, T.; Shelat, A.; Lee, R.E.; Nishiguchi, G.; White, S.W.; Roussel, M.F.; Potts, P.R.; Fischer, M.; Rankovic, Z. Phenyl-Glutarimides: Alternative Cereblon Binders for the Design of PROTACs. *Angew Chem Int Ed Engl* **2021**, *60* (51), 26663-26670.

(27) Xie, S.; Sun, Y.; Liu, Y.; Li, X.; Li, X.; Zhong, W.; Zhan, F.; Zhu, J.; Yao, H.; Yang, D. H.; Chen, Z. S.; Xu, J.; Xu, S. Development of Alectinib-Based PROTACs as Novel Potent Degraders of Anaplastic Lymphoma Kinase (ALK). *J Med Chem* **2021**, *64* (13), 9120-9140.

(28) Whitehouse, A. J.; Thomas, S. E.; Brown, K. P.; Fanourakis, A.; Chan, D. S.; Libardo, M. D. J.; Mendes, V.; Boshoff, H. I. M.; Floto, R. A.; Abell, C.; Blundell, T. L.; Coyne, A. G. Development of

Inhibitors against Mycobacterium abscessus tRNA (m(1)G37) Methyltransferase (TrmD) Using Fragment-Based Approaches. *J Med Chem* **2019**, *62* (15), 7210-7232.

(29) Ma, J.; Luo, J.; Jiang, K.; Zhang, G.; Liu, S.; Yin, B. Access to Polycyclic Thienoindolines via Formal [2+2+1] Cyclization of Alkynyl Indoles with S(8) and K(2)S. *Org Lett* **2021**, *23* (20), 8033-8038.

(30) Spiteri, C.; Moses, J. E. Copper-catalyzed azide-alkyne cycloaddition: regioselective synthesis of 1,4,5-trisubstituted 1,2,3-triazoles. *Angew Chem Int Ed Engl* **2010**, *49* (1), 31-33.

(31) Zerfas, B. L.; Huerta, F.; Liu, H.; Du, G.; Gray, N. S.; Jones, L. H.; Nowak, R. P. Advancing targeted protein degrader discovery by measuring cereblon engagement in cells. *Methods Enzymol* **2023**, *681*, 169-188.

(32) Nowak, R. P.; Ragosta, L.; Huerta, F.; Liu, H.; Ficarro, S. B.; Cruite, J. T.; Metivier, R. J.; Donovan, K. A.; Marto, J. A.; Fischer, E. S.; Zerfas, B. L.; Jones, L. H. Development of a covalent cereblon-based PROTAC employing a fluorosulfate warhead. *RSC Chem Biol* **2023**, *4* (11), 906-912.

(33) Steinebach, C.; Bricelj, A.; Murgai, A.; Sosič, I.; Bischof, L.; Ng, Y. L. D.; Heim, C.; Maiwald, S.; Proj, M.; Voget, R.; Feller, F.; Košmrlj, J.; Sapozhnikova, V.; Schmidt, A.; Zuleeg, M.R.; Lemnitzer, P.; Mertins, P.; Hansen, F. K.; Gütschow, M.; Krönke, J.; Hartmann, M. D. Leveraging Ligand Affinity and Properties: Discovery of Novel Benzamide-Type Cereblon Binders for the Design of PROTACs. *J Med Chem* **2023**, *66* (21), 14513-14543.

(34) Steimbach, R. R.; Herbst-Gervasoni, C. J.; Lechner, S.; Stewart, T. M.; Klinke, G.; Ridinger, J.; Géraldy, M. N. E.; Tihanyi, G.; Foley, J. R.; Uhrig, U.; Kuster, B.; Poschet, G.; Casero Jr., R.A.; Medard, G.; Oehme, I.; Christianson, D. W.; Gunkel, N.; Miller, A. K. Aza-SAHA Derivatives Are Selective Histone Deacetylase 10 Chemical Probes That Inhibit Polyamine Deacetylation and Phenocopy HDAC10 Knockout. *J Am Chem Soc* **2022**, *144* (41), 18861-18875.

(35) Depetter, Y.; Geurs, S.; De Vreese, R.; Goethals, S.; Vandoorn, E.; Laevens, A.; Steenbrugge, J.; Meyer, E.; de Tullio, P.; Bracke, M.; D'Hooghe, M.; De Wever, O. Selective pharmacological inhibitors of HDAC6 reveal biochemical activity but functional tolerance in cancer models. *Int J Cancer* **2019**, *145* (3), 735-747.

(36) Reßing, N.; Schliehe-Diecks, J.; Watson, P. R.; Sonnichsen, M.; Cragin, A. D.; Schöler, A.; Yang, J.; Schäker-Hübner, L.; Borkhardt, A.; Christianson, D. W.; Bhatia, S.; Hansen, F. K. Development of Fluorinated Peptoid-Based Histone Deacetylase (HDAC) Inhibitors for Therapy-Resistant Acute Leukemia. *J Med Chem* **2022**, *65* (22), 15457-15472.

(37) Gadd, M. S.; Testa, A.; Lucas, X.; Chan, K. H.; Chen, W.; Lamont, D. J.; Zengerle, M.; Ciulli, A. Structural basis of PROTAC cooperative recognition for selective protein degradation. *Nat Chem Biol* **2017**, *13* (5), 514-521.

(38) Nowak, R. P.; DeAngelo, S. L.; Buckley, D.; He, Z.; Donovan, K. A.; An, J.; Safaee, N.; Jedrychowski, M. P.; Ponthier, C. M.; Ishoey, M.; Zhang, T.; Mancias, J. D.; Gray, N. S.; Bradner, J. E.; Fischer, E. S. Plasticity in binding confers selectivity in ligand-induced protein degradation. *Nat Chem Biol* **2018**, *14* (7), 706-714.

(39) Drummond, M. L.; Williams, C. I. In Silico Modeling of PROTAC-Mediated Ternary Complexes: Validation and Application. *J Chem Inf Model* **2019**, *59* (4), 1634-1644.

(40) Drummond, M. L.; Henry, A.; Li, H.; Williams, C. I. Improved Accuracy for Modeling PROTAC-Mediated Ternary Complex Formation and Targeted Protein Degradation via New In Silico Methodologies. *J Chem Inf Model* **2020**, *60* (10), 5234-5254.

(41) Li, Y.; Manickam, G.; Ghoshal, A.; Subramaniam, P. More Efficient Palladium Catalyst for Hydrogenolysis of Benzyl Groups. *Synthetic Communications* **2006**, *36* (7), 925-928.

(42) Wang, Y.; Gong, N.; Ma, C.; Zhang, Y.; Tan, H.; Qing, G.; Zhang, J.; Wang, Y.; Wang, J.; Chen, S.; Li, X.; Ni, Q.; Yuan, Y.; Gan, Y.; Chen, J.; Li, F.; Zhang, J.; Ou, C.; Zhao, Y.; Liu, X.; Liang, X. J. An amphiphilic dendrimer as a light-activable immunological adjuvant for in situ cancer vaccination. *Nat Commun* **2021**, *12* (1), 4964.

(43) Kraft, F. B.; Enns, J.; Honin, I.; Engelhardt, J.; Scholer, A.; Smith, S. T.; Meiler, J.; Schäker-Hübner, L.; Weindl, G.; Hansen, F. K. Groebke Blackburn Bienayme-mediated multi-component synthesis of selective HDAC6 inhibitors with anti-inflammatory properties. *Bioorg Chem* **2024**, *143*, 107072.

(44) Schäker-Hübner, L.; Warstat, R.; Ahlert, H.; Mishra, P.; Kraft, F. B.; Schliehe-Diecks, J.; Schöler, A.; Borkhardt, A.; Breit, B.; Bhatia, S.; Hügle, M.; Günther, S.; Hansen, F. K. 4-Acyl Pyrrole Capped HDAC Inhibitors: A New Scaffold for Hybrid Inhibitors of BET Proteins and Histone Deacetylases as Antileukemia Drug Leads. *J Med Chem* **2021**, *64* (19), 14620-14646.

(45) Kraft, F. B.; Hanl, M.; Feller, F.; Schäker-Hübner, L.; Hansen, F. K. Photocaged Histone Deacetylase Inhibitors as Prodrugs in Targeted Cancer Therapy. *Pharmaceuticals (Basel)* **2023**, *16* (3).

(46) Steinebach, C.; Ng, Y. L. D.; Sosič, I.; Lee, C. S.; Chen, S.; Lindner, S.; Vu, L. P.; Bricelj, A.; Haschemi, R.; Monschke, M.; Steinwarz, E.; Wagner, K. G.; Bendas, G.; Luo, J.; Gütschow, M.; Krönke, J. Systematic exploration of different E3 ubiquitin ligases: an approach towards potent and selective CDK6 degraders. *Chem Sci* **2020**, *11* (13), 3474-3486.

(47) Daina, A.; Michielin, O.; Zoete, V. SwissADME: a free web tool to evaluate pharmacokinetics, drug-likeness and medicinal chemistry friendliness of small molecules. *Sci Rep* **2017**, *7*, 42717.

(48) Schäker-Hübner, L.; Haschemi, R.; Buch, T.; Kraft, F. B.; Brumme, B.; Scholer, A.; Jenke, R.; Meiler, J.; Aigner, A.; Bendas, G.; Hansen, F. K. Balancing Histone Deacetylase (HDAC) Inhibition and Drug-likeness: Biological and Physicochemical Evaluation of Class I Selective HDAC Inhibitors.

ChemMedChem **2022**, *17* (9), e202100755.

(49) Sinatra, L.; Vogelmann, A.; Friedrich, F.; Tararina, M. A.; Neuwirt, E.; Colcerasa, A.; König, P.; Toy, L.; Yesiloglu, T. Z.; Hilscher, S.; Gaitzsch, L.; Papenkordt, N.; Zhai, S.; Zhang, L.; Romier, C.; Einsle, O.; Sippl, W.; Schutkowski, M.; Gross, O.; Bendas, G.; Christianson, D. W.; Hansen, F. K.; Jung, M.; Schiedel, M. Development of First-in-Class Dual Sirt2/HDAC6 Inhibitors as Molecular Tools for Dual Inhibition of Tubulin Deacetylation. *J Med Chem* **2023**, *66*, 14787-14814.

(50) Feller, F.; Hansen, F. K. Targeted Protein Degradation of Histone Deacetylases by Hydrophobically Tagged Inhibitors. *ACS Med Chem Lett* **2023**, *14* (12), 1863-1868.

(51) Donovan, K. A.; An, J.; Nowak, R. P.; Yuan, J. C.; Fink, E. C.; Berry, B. C.; Ebert, B. L.; Fischer, E. S. Thalidomide promotes degradation of SALL4, a transcription factor implicated in Duane Radial Ray syndrome. *Elife* **2018**, *7*.

(52) Skowronek, P.; Thielert, M.; Voytik, E.; Tanzer, M. C.; Hansen, F. M.; Willems, S.; Karayel, O.; Brunner, A.-D.; Meier, F.; Mann, M. Rapid and in-depth coverage of the (phospho-) proteome with deep libraries and optimal window design for dia-PASEF. *Mol Cell Proteomics* **2022**, 21, 100279.

(53) Demichev, V.; Messner, C. B.; Vernardis, S. I.; Lilley, K. S.; Ralser, M. DIA-NN: neural networks and interference correction enable deep proteome coverage in high throughput. *Nature methods* **2020**, *17* (1), 41-44.

(54) Ritchie, M. E.; Phipson, B.; Wu, D.; Hu, Y.; Law, C. W.; Shi, W.; Smyth, G. K. limma powers differential expression analyses for RNA-sequencing and microarray studies. *Nucleic Acids Res* **2015**, *43* (7), e47.

Table of Contents Graphic